# Authigenic mineral phases as a driver of the upper ocean iron cycle

Alessandro Tagliabue[1]*, Kristen N. Buck[2,3], Laura E. Sofen[4], Benjamin S. Twining[4], Olivier Aumont[5], Philip W. Boyd[6], Salvatore Caprara[2], William B. Homoky[7], Rod Johnson[8], Daniela König[1], Daniel C. Ohnemus[9], Bettina Sohst[10], Peter Sedwick[10]

1. School of Environmental Sciences, University of Liverpool, L68 3GP, UK
2. College of Marine Science, University of South Florida, Tampa, FL 33620, USA
3. College of Earth, Ocean, and Atmospheric Sciences, Oregon State University, Corvallis, OR 97331, USA
4. Bigelow Laboratory for Ocean Sciences, East Boothbay, ME 04544, USA
5. LOCEAN, IRD-CNRS-Sorbonne Université-MNHN, IPSL, Paris, France
6. Institute for Marine and Antarctic Studies, University of Tasmania, Hobart, Tasmania, Australia
7. School of Earth and Environment, University of Leeds, Leeds, LS2 9JT, UK
8. Bermuda Institute for Ocean Sciences, St. Georges GE01, Bermuda
9. Skidaway Institute of Oceanography, University of Georgia, Dept. of Marine Sciences, Savannah GA, 31404 USA
10. Department of Ocean and Earth Sciences, Old Dominion University, Norfolk, VA 23529, USA

*corresponding author: a.tagliabue@liverpool.ac.uk

**Iron is important in regulating the ocean carbon cycle[1]. Although multiple dissolved and particulate species participate in oceanic iron cycling, current understanding emphasises the importance of complexation by organic ligands in stabilising oceanic dissolved iron concentrations[2-6]. However, it is difficult to reconcile this view of ligands as a primary control on dissolved iron cycling with the observed size partitioning of dissolved iron species, inefficient dissolved iron regeneration at depth or the potential importance of authigenic iron phases in particulate iron observational datasets[7-12]. Here we present a novel dissolved iron, ligand and particulate iron seasonal dataset from the Bermuda Atlantic Time-series Study region. We find that upper-ocean dissolved iron dynamics were decoupled from those of ligands, which necessitates a process by which dissolved iron escapes ligand stabilisation to generate a reservoir of authigenic iron particles that settle to depth. When this "colloidal shunt" mechanism was implemented in a global-scale biogeochemical model, it reproduced both seasonal iron cycle dynamics observations and independent global datasets where previous models failed[13-15]. Overall, we argue that the turnover of authigenic particulate iron phases must be considered alongside biological activity and ligands in controlling ocean dissolved iron distributions and the coupling between dissolved and particulate iron pools.**

Iron (Fe) is an essential element that governs microbial activity over much of the ocean and, via its influence on the biological carbon pump, modulates the carbon cycle[1]. For instance, past changes in Fe supply to the ocean during glacial periods are invoked as a driver of fluctuations in atmospheric carbon dioxide levels[16]. On the early Earth, low oxygen levels meant Fe was abundant and thus utilized as a catalyst for multiple cellular processes in marine phytoplankton, including photosynthesis and respiration[17,18]. As the ocean became oxygenated, ferrous Fe ($Fe^{2+}$) was oxidised to form ferric ($Fe^{3+}$) (oxyhydr)oxides, which would have precipitated or adsorbed to particles and thus become lost from the dissolved Fe (DFe) phase (< 0.2μm) that is most bioavailable to marine phytoplankton[1]. Complexation of ferric Fe by organic molecules, known as ligands, has been thought to stabilise DFe by preventing loss through oxidative precipitation, thereby regulating ocean DFe concentrations[2]. This relatively simple hypothesis has been invoked to explain observations of Fe in the ocean interior[3,5,6], the ocean carbon cycle[19] and the balance between ocean Fe and nitrogen limitation[4]. Syntheses of available ligand and DFe data have shown that ligand concentrations are usually well in excess of DFe[20-22], implying that the complexation capacity of Fe-binding ligands is often undersaturated. However, this finding is at

odds with estimates of substantial DFe removal rates along watermass transport pathways and limited net solubilisation of DFe from remineralisation of sinking particulate Fe (PFe)[7,8,10,23-25]. Global ocean Fe models, parameterised to represent ligand control of DFe, also tend to perform poorly against large-scale ocean DFe datasets[13,14], indicating that our current understanding cannot accurately constrain the ocean Fe cycle. This knowledge gap undermines confidence in projections of the impacts of environmental change in Fe-limited ocean regions[26].

Authigenic mineral phases are known to play an important role in the cycling of Fe in the Earth system, but have so far been largely ignored as a driver of the contemporary ocean Fe cycle[1]. Oxidation of Fe(II) to Fe(III) in natural waters precipitates colloidal-sized (~0.02-0.2μm) Fe (CFe) (oxyhydr)oxides, such as nano-ferrihydrite, -goethite and -haematite, which may also sorb organic carbon functional groups[27] and undergo further aggregation to form sinking authigenic PFe (>0.2μm). Authigenic Fe phases are commonly invoked as significant components of external iron inputs from rivers, sediments, icebergs and hydrothermal vents[e.g.28-30] and CFe may comprise 50% or more of the ocean DFe pool, depending on the environmental setting[31,32]. Yet despite their ubiquity, how aggregation of colloidal iron oxides to form sinking authigenic PFe and regulates Fe cycling alongside ligand stabilisation is unknown, especially as Fe is not equally exchanged between the colloidal and ligand-bound dissolved pools[11,12]. In the particulate phase, authigenic Fe phases can be important[9] and have been estimated to account for as much as 40% of total PFe in the south Pacific[10] and Ross Sea[33]. Care is needed when deriving large-scale corrections for lithogenic PFe, but an examination of chemically-labile PFe observations from the recent GEOTRACES IDP2021 suggests that between half and three quarters of samples have PFe that cannot be accounted for as biogenic PFe (typically assumed to be the major labile pool, see Methods). Taken together, these observations imply that we may be neglecting a crucial component in our understanding of the ocean iron cycle.

A critical challenge in Earth science is to quantify the response of ocean systems to environmental change. This is particularly acute for iron, which has a short residence time and is thus responsive to rapid alterations to ocean physics and atmospheric inputs (e.g. from anthropogenic activity[34] and wildfires[35]). Although the database of oceanic DFe observations has grown markedly during the multi-decadal GEOTRACES global survey, we lack insight into concurrent temporal variations in dissolved, ligand-bound and particulate Fe (Extended Data Table 1), which constitute a robust test for hypotheses regarding the mechanisms driving the Fe cycle[eg7,36]. The degree to which DFe inventories are controlled by ligands and/or authigenic phases is not testable with currently available data. Addressing this issue is important because it hampers our understanding of the mechanisms that drive oceanic Fe distributions and therefore the ocean carbon cycle and marine ecosystems. Here we report a new seasonal-scale Fe observational dataset (the Bermuda Atlantic Iron Time-series, BAIT) comprising the parallel seasonal evolution of DFe, ligands and PFe phases in the Bermuda Atlantic Time-series Study (BATS) region of the Sargasso Sea, designed to explore these drivers in an integrated fashion for the first time. Together these data yield a new conceptual and numerical model of the ocean Fe cycle that uniquely reconciles the roles of biological activity, ligands and authigenic phases, with important implications for the global ocean Fe and carbon cycles.

**Seasonal dissolved iron and ligand variations**

We conducted fieldwork in March, May, August and November 2019, sampling the BATS site and two adjacent spatial stations to ~1,800 m depth each time, and observed a pronounced seasonal cycle in the upper-ocean DFe inventory, consistent with prior observations[15]. Aeolian deposition drove an increase in surface DFe concentrations from low levels (~0.08-0.22 nM) in late-winter (March) to values over 1.5 nM in late summer (August), decreasing to ~0.5 nM by late fall (November; Figure 1). Notably, despite the sub-tropical location of the BATS region, these low winter DFe concentrations are more typical of the strongly Fe-limited Southern Ocean[37]. In contrast to the upper ocean, there was little seasonal change below depths of ~1000 m, where DFe

concentrations remained around 0.75-1 nM (Figure 1), similar to other regional datasets[15,38,39]. Integrated over the upper 200 m that encompasses the seasonal thermocline, DFe inventories increase almost three-fold, from 30 µmol $m^{-2}$ in March to 70 µmol $m^{-2}$ in August, before decreasing to just below 50 µmol $m^{-2}$ in November (Figure 2a). Horizontal changes during this study, driven by the regional eddy field[15], were small relative to the seasonal dynamics (as seen by the strong similarity and low standard error across the three profiles per voyage). Consistent with its location in the North Atlantic subtropical gyre, net biological removal of Fe at BATS is low[40].

Importantly, high turnover in the DFe inventories took place against the backdrop of a strong excess Fe-complexation capacity in both total- and stronger Fe-binding ligands. In the upper 200 m, we provide the first evidence that concentrations of total and strong Fe-binding ligands (LT and L1, respectively, see Methods) consistently exceeded DFe concentrations by ~3 nM and ~1 nM throughout the year (Extended Data Figures 1 and 2). Below 1000 m, the excesses in stronger ligands dropped below 0.5 nM, whereas those of the weaker total ligands remained more than 1 nM above DFe concentrations. Integrated over the upper 200 m, inventories of total and stronger ligands showed much smaller seasonal changes, and remained 2- to 5-fold in excess of DFe year round (integrated inventories always exceeded 450 or 200 µmol $m^{-2}$ for total and stronger ligands, respectively; Figure 2a).

This seasonal evolution of DFe and ligands, documented here for the first time, cannot be reproduced by a global ocean model that assumes equilibrium between DFe and ligands. The PISCES-Quota global model accounts for a complex representation of the ocean Fe cycle, including lithogenic particles and ligand stabilisation of DFe. Total weaker ligand concentrations were derived from dissolved organic carbon (DOC) or modelled as stronger ligands and matched observations well (Figure 2b, Extended Data Figure 1, Methods). Thus the PISCES-Quota model serves as a direct test of whether the seasonal observations of DFe could be reproduced with accurate representation of ligands. Across a range of total ligand-to-DOC ratios or with stronger ligands, PISCES-Quota performed well in reproducing observed DFe concentrations below 1000m, but systematically overestimated upper ocean DFe concentrations (black lines in Figure 1).

PISCES-Quota model experiments failed to generate sufficient excesses in total or stronger ligands, relative to observations (Extended Data Figure 2), because greater concentrations of ligands in the model lead to excessive DFe. Comparing the modelled seasonal variations in the inventories of DFe and ligands side by side, we find a strong link emerges (Figure 2c), as expected from the posited conceptual coupling of DFe and ligands[4]. However, the observed contemporaneous evolution of the DFe and ligand inventories do not conform to this expectation (for either stronger or total weaker ligands, Figure 2c). This indicates an assumed equilibrium between ligands and DFe is not compatible with our observations in the upper water column. This poor skill for DFe is not unusual for global ocean Fe models[8], but its persistence here implies that it does not arise from errors in the representation of Fe-binding ligands. Moreover, alternative approaches, such as applying greater scavenging rate on DFe by lithogenic particles suggested previously[41] does not improve the model-observation fit either (Extended Data Figure 3) and biological removal of iron is low (see below). This suggests that the prevailing Fe-ligand stabilisation theory is insufficient to explain our new observations.

**Reconciling observations and models**

To reconcile our observations, we advance a new conceptual model that decouples the cycling of Fe through CFe (oxyhydr)oxides from dissolved organic ligands, building on ideas developed for thorium[42]. However, instead of assuming metals adsorb onto colloidal organic matter, we focus here on the aggregation of CFe (oxyhyr)oxides: CFe is observed to be a significant component of DFe, often making up more than 50% in our samples, and accumulated seasonally in the upper 200 m (similar to other work in this region[31,32,43]). Unlike the few previous models that include CFe[44] or explore dissolved-particulate partitioning[45], and in agreement with estimates from

thermodynamic partitioning work[11,12] and porewater modelling[29], we assume that CFe (part of the <0.2 µm DFe pool) is *not* chemically complexed by ligands. Instead, CFe is considered to be comprised of Fe oxyhydroxide minerals that aggregate with bulk DOC to produce small authigenic particles that aggregate into larger authigenic particles (both within the >0.2 µm PFe pool), which then sink and cycle independently of ligand-bound DFe (see Methods, Figure 2d). As previously, ligand dynamics in this new model assume either prescribed weaker total ligands or prognostically simulated stronger ligands driven by specific source-sink dynamics (either approach fits observations well, Extended Data Figure 1, see Methods). Our new PISCES-Quota-Fe model shows a dramatically improved ability to reproduce our seasonal observations of DFe (Figure 1), excess ligands (Extended Data Figure 2) and the evolution of upper 200m DFe and ligand inventories (Figure 2c). These improvements are striking considering the dynamics of the seasonal cycle at the BATS site, particularly the excellent fit by season and depth, compared to prior efforts[13-15]. Overall, PISCES-Quota-Fe results were insensitive to whether we chose to model total weaker or stronger ligands. This indicates that while ligands are critical to stabilise the soluble (<0.02 µm) portions of the DFe pool, additional mechanisms are required to explain the fate of CFe. Greater emphasis on the cycling of CFe (oxyhydr)oxides and authigenic Fe minerals (as part of the PFe pool) as first order drivers of the upper ocean DFe cycle is required.

Observed and modelled authigenic PFe concentrations provide further support for the importance of CFe cycling. An important corollary of our new conceptual viewpoint is that if CFe (oxyhydr)oxides are not in equilibrium with organic Fe-binding ligands, then authigenic PFe should accumulate alongside the more commonly considered lithogenic and biogenic PFe pools. We measured total PFe in samples from each BAIT voyage and derived the authigenic contribution by subtracting the lithogenic and biogenic components of PFe, using a variety of approaches (see Methods)[10]. Overall, between 15-56% and 20-62% of the total PFe was authigenic (i.e. not accounted for by biogenic or lithogenic pools) in the upper 200 m and the 200-2000 m depth strata, respectively (Figure 3), consistent with limited prior indications[10] . Strikingly, estimates of lithogenic, biogenic and authigenic PFe from our new PISCES-Quota-Fe global model closely match observations, both in terms of overall magnitude, seasonal changes, and the increase in authigenic PFe with depth (Figure 3). This further model-data convergence bolsters our hypothesis regarding the importance of Fe cycling through CFe (oxhydr)oxides “colloidal shunt” that is not in equilibrium with dissolved Fe-binding organic ligands. The small magnitude of the biogenic PFe pool also emphasises the key role for non-biogenic processes in regulating the upper ocean Fe inventory.

Globally, PISCES-Quota-Fe displays improved skill for both DFe and PFe observations. Across >10,000 and >1,500 observations for DFe and PFe, respectively, PISCES-Quota shows a reduced bias and a better correlation and slope, both throughout the water column and in the upper 200m (Extended Data Table 2, Extended Data Figure 4). PISCES-Quota-Fe is also able to retain the existing skill of the PISCES-Quota model in reproducing the distributions of a broad suite of biogeochemical tracers, including nutrients, oxygen, chlorophyll and particulate organic carbon export (Extended Data Figure 5), similar to other earth system models[46].

**A new view of global ocean Fe cycling**

The upper ocean Fe cycle modulates biological activity and the biological C pump. Our results reveal a delicate balance between ligand stabilisation, biological cycling by the “ferrous wheel”, and abiotic cycling through authigenic phases via the newly emphasised “colloidal shunt” in regulating Fe cycling (Figure 4a). Their relative role can be quantified using our new PISCES-Quota-Fe model (Figure 4, using discrete inventories). Where biological activity is high (e.g. parts of the Southern Ocean or eastern boundary upwelling systems), the biological ferrous wheel dominates (~23% of the ocean surface area), as in prior studies[7]. Where total Fe concentrations and biological activity are lower (e.g. the remote oligotrophic gyres of the Pacific Ocean), ligand stabilisation of Fe dominates (~18% of ocean area). Wherever Fe inputs are increased (e.g. below the Saharan dust plume or along the Antarctic coastline), Fe is predominantly cycled through the

colloidal shunt (~40% of ocean area). In around one fifth of the surface ocean (white areas), multiple processes are important. Overall, a mosaic of factors that compete for available Fe in the surface ocean. In the ocean interior, scavenging and regeneration are considered as the dominant drivers[10,23,38]. However, our results introduce Fe (oxyhydr)oxide aggregation and authigenic PFe disaggregation as additional key sinks and sources of DFe, respectively, especially in the interior of the Atlantic and Southern Oceans, where they reach or exceed 50% of the total Fe source or sink fluxes (Extended Data Figure 6). The balance between authigenic PFe production and dissolution will dictate how much of the authigenic particle export, initiated by the colloidal shunt, replenishes deep ocean DFe levels or is removed to the sediments. Further constraints on the underlying processes will improve our understanding of their relative magnitudes and sensitivity to change.

Authigenic Fe phases in the open ocean are likely dominated by mixed Fe (oxyhdr)oxides, including ferrihydrite, goethite and magnetite[28,47,48]. Understanding how these, and potentially other mineral phases, may contribute to differences in the reactivity, solubility, and affinity for organic carbon will illuminate their contribution to ocean Fe and carbon cycling. This will be especially true if the findings from marine sediments and porewaters that organic C stabilises Fe (oxyhdr)oxide colloids[29] and that Fe-minerals enhance preservation of organic C[49], also apply in the water column. Resolving these questions requires additional experimental and process study efforts, integrated with ocean modelling, to deliver the missing mechanistic understanding. Although Fe (oxyhydr)oxides form readily in today's oxic ocean, it is possible that during past or future periods of lower ocean oxygen, the formation of Fe (oxyhydr)oxides would be diminished and the importance of the colloidal shunt may be lessened, with a stronger role for ligands and biological cycling. This new view of the ocean Fe cycle has multiple far reaching implications for DFe removal pathways, surface ocean Fe limitation, sediment-ocean coupling and presents new linkages between the Fe and carbon cycles.

**Acknowledgements**

We thank the Captains and crews of RV *Atlantic Explorer* and RV *Endeavor*, and the BATS program team, for their invaluable assistance during the four project cruises. Olga Antipova provided assistance in synchrotron data collection and analysis and Shannon Burns provided assistance with sampling at sea. The model simulations were undertaken on Barkla, part of the High Performance Computing facilities at the University of Liverpool, UK. AT and DK were supported by NERC award NE/S013547/1; PS and BS were supported by NSF award OCE-1829833; BST, DCO, and LES were supported by NSF award OCE-1829819; KB and SC were supported by NSF award OCE-1829777; RJ was supported by NSF award OCE-1829844. This research used resources of the Advanced Photon Source, a U.S. Department of Energy (DOE) Office of Science user facility operated for the DOE Office of Science by Argonne National Laboratory under Contract No. DE-AC02-06CH11357. We extend our thanks to three reviewers whose comments helped improve the final manuscript.

**Author Contributions**

The overarching BAIT programme was conceptualised by PS, KNB, RJ, AT, DCO and BST. Field and laboratory work was conducted by KNB, SC, RJ, DCO, LES, BS, PS, AT and BST. This study was designed and led by AT, alongside KNB, LES and BST, with further contributions from OA, PWB, WBH and PS. Analysis of dissolved iron, ligands and particles was performed by PS and BS, KNB and SC, and LES and BST, respectively. Modelling work was undertaken by AT. Data synthesis and model-data comparisons were conducted by AT, DK and LES. AT led the drafting of the manuscript with input from all co-authors.

**Data Availability statement** Oceanographic data collected and analysed in this study are available here: https://www.bco-dmo.org/project/822807 and here: https://www.bco-dmo.org/dataset/888772

**Code Availability statement** Model code is available here: https://github.com/atagliab/PISCES-BAIT and output here: https://doi.org/10.5281/zenodo.7378193

**Competing interests** The authors declare no competing interests.

## References


1 Tagliabue, A. et al. The integral role of iron in ocean biogeochemistry. Nature 543, 51-59, doi:10.1038/nature21058 (2017).

2 Gledhill, M. & Buck, K. N. The organic complexation of iron in the marine environment: a review. Frontiers in microbiology 3, 69, doi:10.3389/fmicb.2012.00069 (2012).

3 Johnson, K. S., Gordon, R. M. & Coale, K. H. What controls dissolved iron concentrations in the world ocean? Marine Chemistry 57, 137-161, doi:10.1016/s0304-4203(97)00043-1 (1997).

4 Lauderdale, J. M., Braakman, R., Forget, G., Dutkiewicz, S. & Follows, M. J. Microbial feedbacks optimize ocean iron availability. Proceedings of the National Academy of Sciences of the United States of America 117, 4842-4849, doi:10.1073/pnas.1917277117 (2020).

5 Parekh, P., Follows, M. J. & Boyle, E. A. Decoupling of iron and phosphate in the global ocean. Global Biogeochemical Cycles 19, doi:10.1029/2004gb002280 (2005).

6 Whitby, H. et al. A call for refining the role of humic-like substances in the oceanic iron cycle. Sci Rep 10, 6144, doi:10.1038/s41598-020-62266-7 (2020).

7 Boyd, P. W., Ellwood, M. J., Tagliabue, A. & Twining, B. S. Biotic and abiotic retention, recycling and remineralization of metals in the ocean. Nature Geoscience 10, 167-173, doi:10.1038/ngeo2876 (2017).

8 Frew, R. D. et al. Particulate iron dynamics during FeCycle in subantarctic waters southeast of New Zealand. Global Biogeochemical Cycles 20, doi:10.1029/2005gb002558 (2006).

9 Ohnemus, D. C., Torrie, R. & Twining, B. S. Exposing the distributions and elemental associations of scavenged particulate phases in the ocean using basin-scale multi-element datasets. Global Biogeochemical Cycles, doi:10.1029/2018gb006145 (2019).

10 Tagliabue, A. et al. The interplay between regeneration and scavenging fluxes drives ocean iron cycling. Nature communications 10, 4960, doi:10.1038/s41467-019-12775-5 (2019).

11 Cullen, J. T., Bergquist, B. A. & Moffett, J. W. Thermodynamic characterization of the partitioning of iron between soluble and colloidal species in the Atlantic Ocean. Marine Chemistry 98, 295-303, doi:10.1016/j.marchem.2005.10.007 (2006).

12 Fitzsimmons, J. N., Bundy, R. M., Al-Subiai, S. N., Barbeau, K. A. & Boyle, E. A. The composition of dissolved iron in the dusty surface ocean: An exploration using size-fractionated iron-binding ligands. Marine Chemistry 173, 125-135, doi:10.1016/j.marchem.2014.09.002 (2015).

13 Tagliabue, A. et al. How well do global ocean biogeochemistry models simulate dissolved iron distributions? Global Biogeochemical Cycles, doi:10.1002/2015gb005289 (2016).

14 Somes, C. J. et al. Constraining Global Marine Iron Sources and Ligand-Mediated Scavenging Fluxes With GEOTRACES Dissolved Iron Measurements in an Ocean Biogeochemical Model. Global Biogeochemical Cycles 35, doi:10.1029/2021gb006948 (2021).

15 Sedwick, P. N. et al. Dissolved iron in the Bermuda region of the subtropical North Atlantic Ocean: Seasonal dynamics, mesoscale variability, and physicochemical speciation. Marine Chemistry, doi:10.1016/j.marchem.2019.103748 (2020).

16 Martinez-Garcia, A. et al. Iron fertilization of the Subantarctic ocean during the last ice age. Science 343, 1347-1350, doi:10.1126/science.1246848 (2014).

17 Raven, J. A., Evans, M. C. W. & Korb, R. E. The role of trace metals in photosynthetic electron transport in O2-evolving organisms. Photosynthesis research 60, 111-150, doi:10.1023/a:1006282714942 (1999).

18 Wade, J., Byrne, D. J., Ballentine, C. J. & Drakesmith, H. Temporal variation of planetary iron as a driver of evolution. Proceedings of the National Academy of Sciences of the United States of America 118, doi:10.1073/pnas.2109865118 (2021).

19 Tagliabue, A., Aumont, O. & Bopp, L. The impact of different external sources of iron on the global carbon cycle. Geophysical Research Letters 41, 920-926, doi:10.1002/2013gl059059 (2014).

20 Buck, K. N., Sedwick, P. N., Sohst, B. & Carlson, C. A. Organic complexation of iron in the eastern tropical South Pacific: Results from US GEOTRACES Eastern Pacific Zonal Transect (GEOTRACES cruise GP16). Marine Chemistry, doi:10.1016/j.marchem.2017.11.007 (2017).

21 Buck, K. N., Sohst, B. & Sedwick, P. N. The organic complexation of dissolved iron along the U.S. GEOTRACES (GA03) North Atlantic Section. Deep Sea Research Part II: Topical Studies in Oceanography 116, 152-165, doi:10.1016/j.dsr2.2014.11.016 (2015).
22 Gerringa, L. J. A., Rijkenberg, M. J. A., Schoemann, V., Laan, P. & de Baar, H. J. W. Organic complexation of iron in the West Atlantic Ocean. Marine Chemistry 177, 434-446, doi:10.1016/j.marchem.2015.04.007 (2015).
23 Bressac, M. et al. Resupply of mesopelagic dissolved iron controlled by particulate iron composition. Nature Geoscience, doi:10.1038/s41561-019-0476-6 (2019).
24 Lamborg, C. H. et al. The flux of bio- and lithogenic material associated with sinking particles in the mesopelagic “twilight zone” of the northwest and North Central Pacific Ocean. Deep Sea Research Part II: Topical Studies in Oceanography 55, 1540-1563, doi:10.1016/j.dsr2.2008.04.011 (2008).
25 Twining, B. S. et al. Differential remineralization of major and trace elements in sinking diatoms. Limnol. Oceanogr 59, 689-704, doi:10.4319/lo.2014.59.3.0689 (2014).
26 Tagliabue, A. et al. Persistent uncertainties in ocean net primary production climate change projections. Front. Clim. - Predictions and Projections, doi:10.3389/fclim.2021.738224 (2021).
27 Gunnars, A., Blomqvist, S., Johansson, P. & Andersson, C. Formation of Fe(III) oxyhydroxide colloids in freshwater and brackish seawater, with incorporation of phosphate and calcium. Geochimica et Cosmochimica Acta 66, 745-758, doi:10.1016/s0016-7037(01)00818-3 (2002).
28 Feely, R. A., Trefry, J. H., Massoth, G. J. & Metz, S. A comparison of the scavenging of phosphorus and arsenic from seawater by hydrothermal iron oxyhydroxides in the Atlantic and Pacific Oceans. Deep Sea Research Part A. Oceanographic Research Papers 38, 617-623, doi:10.1016/0198-0149(91)90001-v (1991).
29 Homoky, W. B. et al. Iron colloids dominate sedimentary supply to the ocean interior. Proceedings of the National Academy of Sciences of the United States of America 118, doi:10.1073/pnas.2016078118 (2021).
30 Homoky, W. B. et al. Iron and manganese diagenesis in deep sea volcanogenic sediments and the origins of pore water colloids. Geochimica et Cosmochimica Acta 75, 5032-5048, doi:10.1016/j.gca.2011.06.019 (2011).
31 Fitzsimmons, J. N. & Boyle, E. A. Both soluble and colloidal iron phases control dissolved iron variability in the tropical North Atlantic Ocean. Geochimica et Cosmochimica Acta 125, 539-550, doi:10.1016/j.gca.2013.10.032 (2014).
32 Kunde, K. et al. Iron Distribution in the Subtropical North Atlantic: The Pivotal Role of Colloidal Iron. Global Biogeochemical Cycles 33, 1532-1547, doi:10.1029/2019gb006326 (2019).
33 Marsay, C. M., Barrett, P. M., McGillicuddy, D. J. & Sedwick, P. N. Distributions, sources, and transformations of dissolved and particulate iron on the Ross Sea continental shelf during summer. Journal of Geophysical Research: Oceans 122, 6371-6393, doi:10.1002/2017jc013068 (2017).
34 Conway, T. M. et al. Tracing and constraining anthropogenic aerosol iron fluxes to the North Atlantic Ocean using iron isotopes. Nature communications 10, 2628, doi:10.1038/s41467-019-10457-w (2019).
35 Tang, W. et al. Widespread phytoplankton blooms triggered by 2019-2020 Australian wildfires. Nature 597, 370-375, doi:10.1038/s41586-021-03805-8 (2021).
36 Boyd, P. W., Mackie, D. S. & Hunter, K. A. Aerosol iron deposition to the surface ocean - Modes of iron supply and biological responses. Marine Chemistry 120, 128-143, doi:10.1016/J.Marchem.2009.01.008 (2010).
37 Bowie, A. R. et al. Biogeochemical iron budgets of the Southern Ocean south of Australia: Decoupling of iron and nutrient cycles in the subantarctic zone by the summertime supply. Global Biogeochemical Cycles 23, doi:10.1029/2009gb003500 (2009).
38 Wu, J. & Boyle, E. Iron in the Sargasso Sea: Implications for the processes controlling dissolved Fe distribution in the ocean. Global Biogeochemical Cycles 16, 33-31-33-38, doi:10.1029/2001gb001453 (2002).

39 Rijkenberg, M. J. et al. The distribution of dissolved iron in the West Atlantic Ocean. Plos One 9, e101323, doi:10.1371/journal.pone.0101323 (2014).
40 Black, E. E. et al. Ironing Out Fe Residence Time in the Dynamic Upper Ocean. Global Biogeochemical Cycles 34, doi:10.1029/2020gb006592 (2020).
41 Wagener, T., Guieu, C. & Leblond, N. Effects of dust deposition on iron cycle in the surface Mediterranean Sea: results from a mesocosm seeding experiment. Biogeosciences 7, 3769-3781, doi:Doi 10.5194/Bg-7-3769-2010 (2010).
42 Honeyman, B. D. & Santschi, P. H. A Brownian-pumping model for oceanic trace metal scavenging: Evidence from Th isotopes. Journal of Marine Research 47, 951-992, doi:10.1357/002224089785076091 (1989).
43 Wu, J., Boyle, E., Sunda, W. & Wen, L. S. Soluble and colloidal iron in the oligotrophic North Atlantic and North Pacific. Science 293, 847-849, doi:10.1126/science.1059251 (2001).
44 Völker, C. & Tagliabue, A. Modeling organic iron-binding ligands in a three-dimensional biogeochemical ocean model. Marine Chemistry 173, 67-77, doi:10.1016/j.marchem.2014.11.008 (2015).
45 Misumi, K. et al. Slowly Sinking Particles Underlie Dissolved Iron Transport Across the Pacific Ocean. Global Biogeochemical Cycles 35, doi:10.1029/2020gb006823 (2021).
46 Seferian, R. et al. Tracking Improvement in Simulated Marine Biogeochemistry Between CMIP5 and CMIP6. Curr Clim Change Rep, 1-25, doi:10.1007/s40641-020-00160-0 (2020).
47 Raiswell, R., Benning, L. G., Tranter, M. & Tulaczyk, S. Bioavailable iron in the Southern Ocean: the significance of the iceberg conveyor belt. Geochemical transactions 9, 7, doi:10.1186/1467-4866-9-7 (2008).
48 von der Heyden, B. P., Roychoudhury, A. N., Mtshali, T. N., Tyliszczak, T. & Myneni, S. C. Chemically and geographically distinct solid-phase iron pools in the Southern Ocean. Science 338, 1199-1201, doi:10.1126/science.1227504 (2012).
49 Curti, L. et al. Carboxyl-richness controls organic carbon preservation during coprecipitation with iron (oxyhydr)oxides in the natural environment. Communications Earth & Environment 2, doi:10.1038/s43247-021-00301-9 (2021).

## Figure Legends

**Figure 1. Seasonal evolution of dissolved iron** DFe data and model solutions at the BATS site for March, May, August and November. Red crosses are DFe data for each voyage for three stations in the BATS region. Thick and dashed black lines are model solutions at BATS from the standard PISCES-Quota model, with varying total ligands derived from DOC (using 0.09, 0.08 and 0.07 (nM Lt) (µM DOC)$^{-1}$) or, in thin red lines, with prognostic stronger ligands (see Methods). Blue lines represent model solutions from new PISCES-Quota-Fe model accounting for iron oxides and authigenic phases, with either prognostic stronger ligands (solid blue lines, see Methods) or DOC-derived total ligands (dashed blue lines, using 0.09 nM Lt µM DOC$^{-1}$).

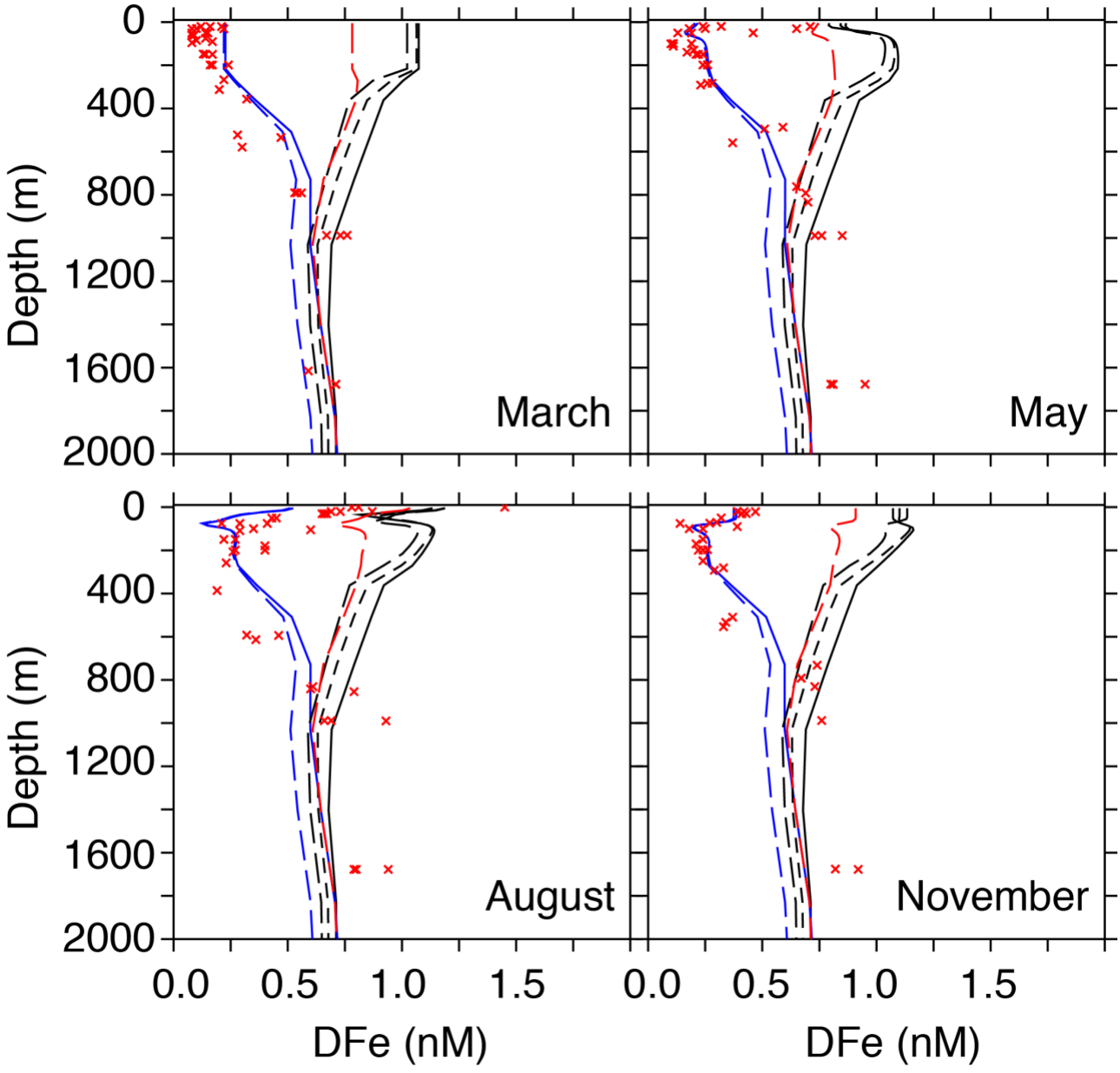

**Figure 2. Observations and modelling of dissolved iron and ligand dynamics** a) Seasonal evolution of DFe and LT or L1 in the upper 200 m from observations ($10^{-6}$ mol $m^{-3}$, error bars represent standard errors across the three stations). b) schematic of the PISCES-Quota model, with all the DFe pool in equilibrium with ligands (as FeL). c) the cross plot of the seasonal evolution of weaker total ligands (LT, pink) or stronger ligands (L1, green) and DFe in the upper 200m. Black symbols represent the solution of the PISCES-Quota model with varying total ligands derived from DOC (using 0.09, 0.08 and 0.07 nM LT µM $DOC^{-1}$) or prognostic stronger ligands (red), while blue symbols represent the solution of the PISCES-Quota-Fe model with either prognostic stronger ligands or DOC derived total ligands (using 0.09 nM Lt µM $DOC^{-1}$). Dashed lines in panel c represent the 1:1 DFe:ligand line and the 0.5:1 DFe:ligand line. d) Schematic of the new PISCES-Quota-Fe model, where only soluble Fe (sFe) is in equilibrium with ligands (as sFeL) and Fe (oxyhyr)oxides ($CFe_{OX}$) aggregate with organic carbon (Corg) to form small and large authigenic Fe particles ($aFe_S$ and $aFe_L$, respectively). The triangle in panels b and d represents the portion of the DFe pool in equilibrium with ligands. The vertical dashed line in panel d represents the boundary between dissolved (<0.2 µm) and particulate Fe (> 0.2 µm).

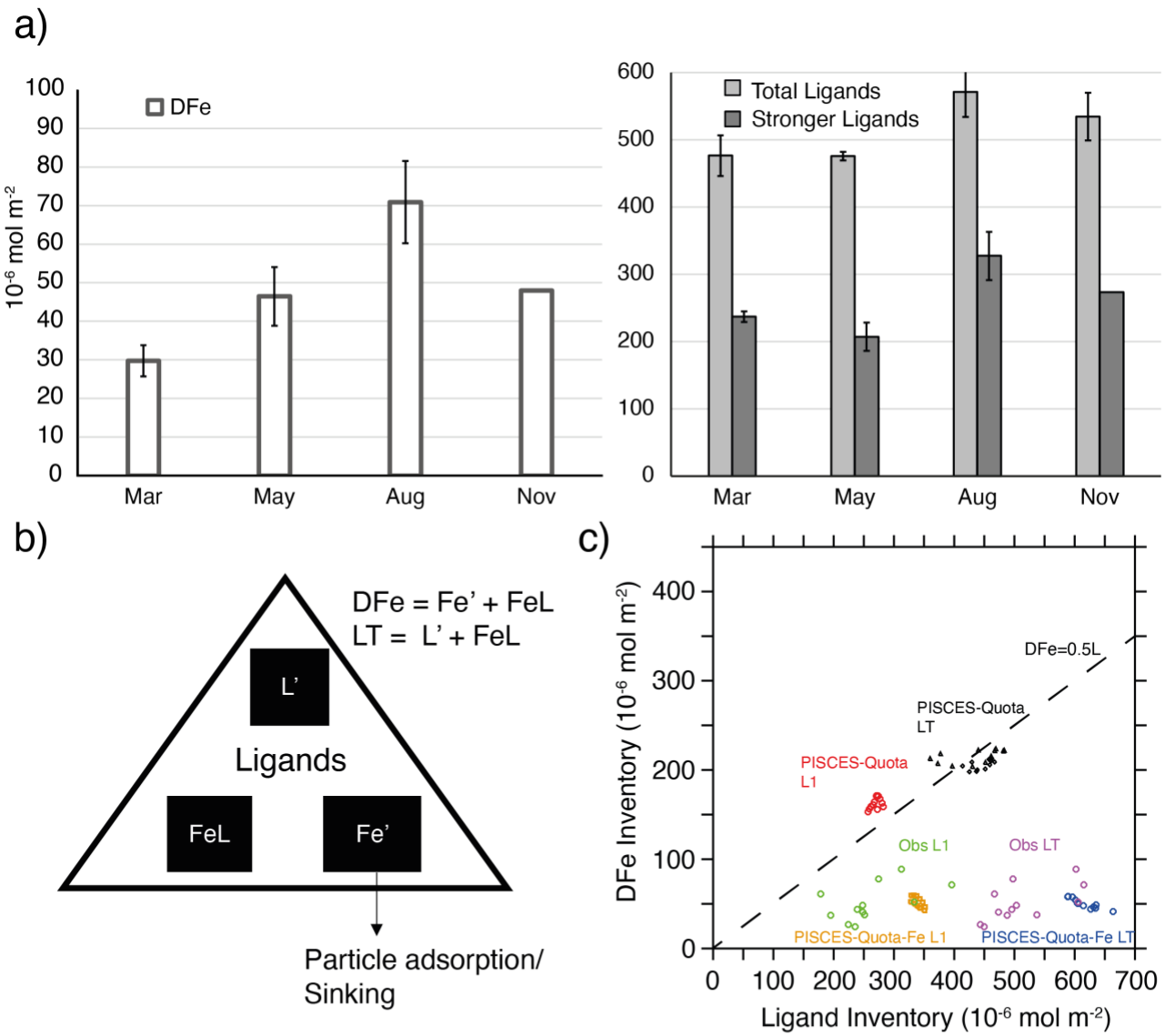
a)
DFe
$10^{-6}$ mol $m^{-2}$
Mar
May
Aug
Nov
Total Ligands
Stronger Ligands
b)
DFe = Fe' + FeL
LT = L' + FeL
L'
Ligands
FeL
Fe'
Particle adsorption/
Sinking
c)
DFe Inventory ($10^{-6}$ mol $m^{-2}$)
Ligand Inventory ($10^{-6}$ mol $m^{-2}$)
DFe=0.5L
PISCES-Quota LT
PISCES-Quota L1
Obs L1
Obs LT
PISCES-Quota-Fe L1
PISCES-Quota-Fe LT
d)
DFe = SFe' + SFeL + $CFe_{OX}$
LT = L' + SFeL
L'
SFeL
SFe'
$CFe_{OX}$
Aggregation
Corg
Disag.
Aggregation/
Disaggregation
$aFe_S$
$aFe_L$
Sinking
Particle adsorption/
Sinking
Dissolved
< 0.2 um
Particulate
> 0.2 um

**Figure 3. Seasonal evolution of particulate iron phases** Lithogenic, authigenic and biogenic PFe phases ($PFe_{Lith}$, $PFe_{Auth}$ and $PFe_{Bio}$, respectively). Lithogenic PFe (in orange) is estimated via three approaches (from left bar to right bar: refractory PFe, using particulate Al and a local Fe:Al ratio and using particulate Al and a standard upper continental crust Fe:Al ratio, see Methods). Biogenic PFe (in green) is estimated using observed Fe cell quotas via particulate phosphorus. Authigenic PFe (in blue) is calculated as the residual from PFe – $PFe_{Lith}$ – $PFe_{Bio}$, with the three estimates spanning the three different $PFe_{lith}$ estimates. Bars without dashes are observations and dashed bars are the solution of the PISCES-Quota-Fe model with prognostic stronger ligands at the BATS site for each of the months concerned. The error bars on the observations represent the standard error across the three stations sampled each cruise.

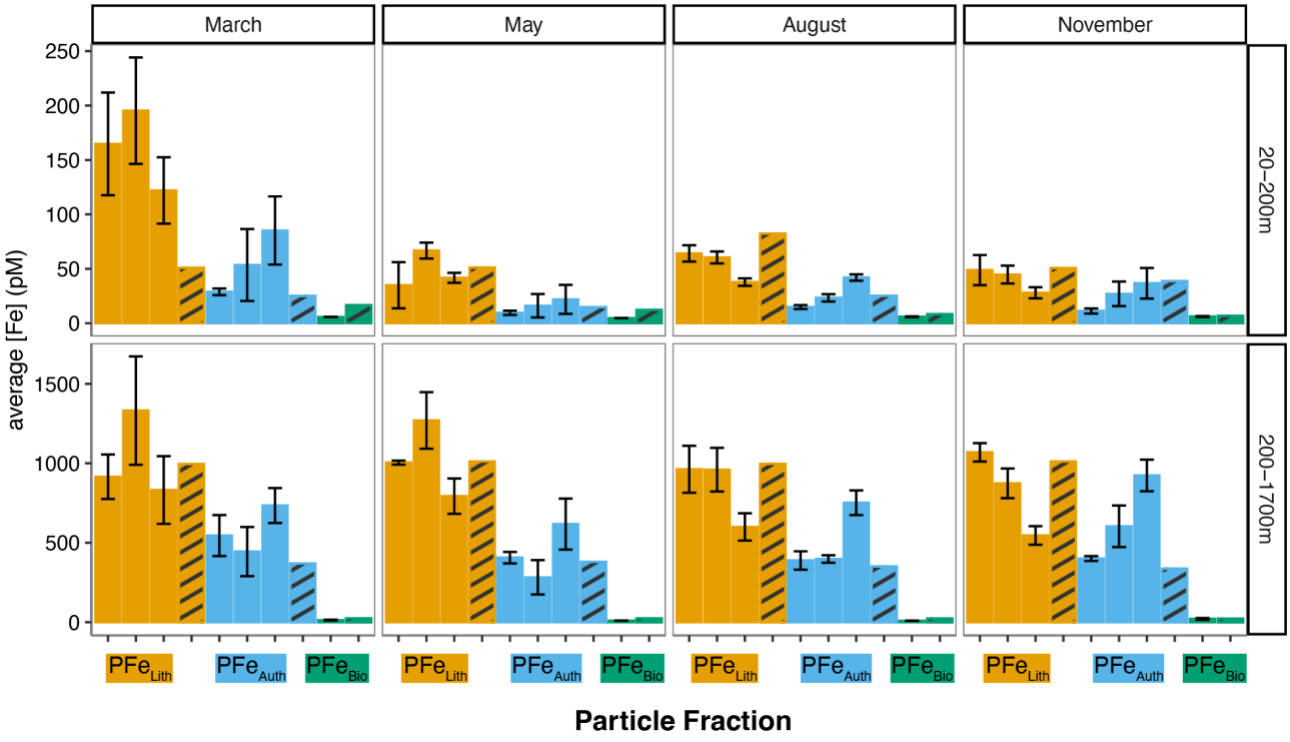

458 **Figure 4. An integrated view of the ocean iron cycle** (a) A schematic illustrating how the
459 biological uptake (green: sum of diatom, picophytoplankton, nanophytoplankton, microzooplankton,
460 mesozooplankton and organic particulate Fe), ligand stabilisation (blue: sum of organically
461 complexed and free dFe) and the colloidal shunt (orange: sum of colloidal iron (oxyhydr)oxides and
462 small and large authigenic particle Fe) maintain surface ocean Fe levels. Panel b) shows model
463 quantifications of the dominant term at each location using the new PISCES-Quota-Fe model in
464 the same colours, with white areas denoting regions where more than one process dominates.
465

a)

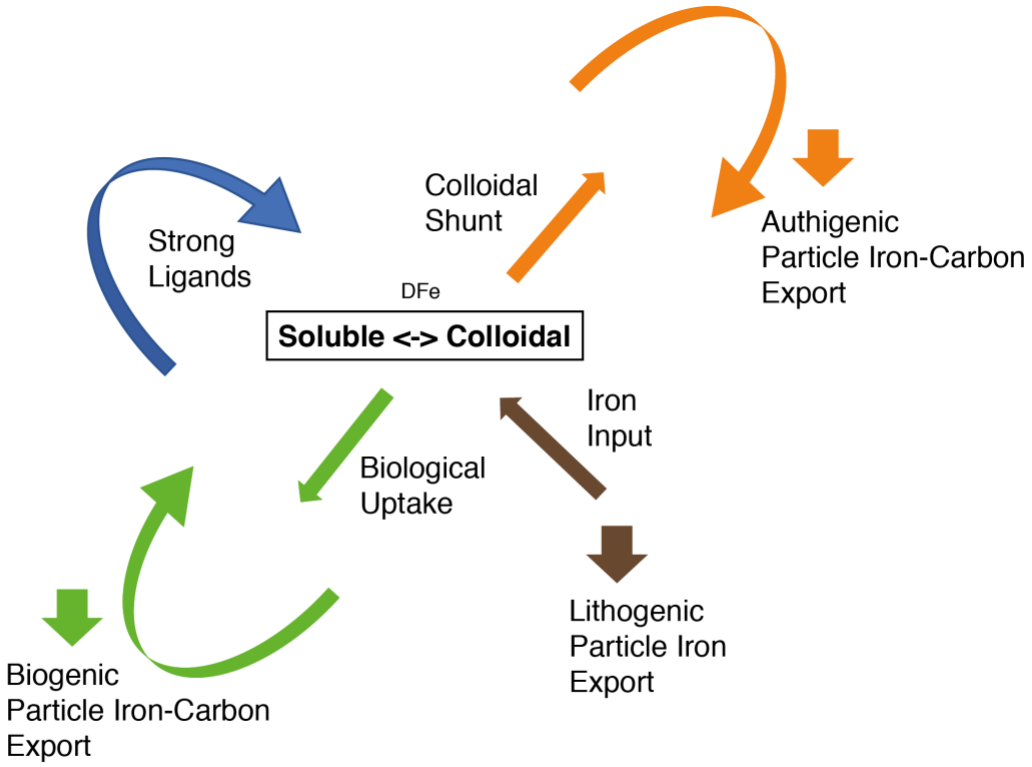
Colloidal
Shunt
Strong
Ligands
Authigenic
Particle Iron-Carbon
Export
DFe
Soluble <-> Colloidal
Iron
Input
Biological
Uptake
Lithogenic
Particle Iron
Export
Biogenic
Particle Iron-Carbon
Export

b)

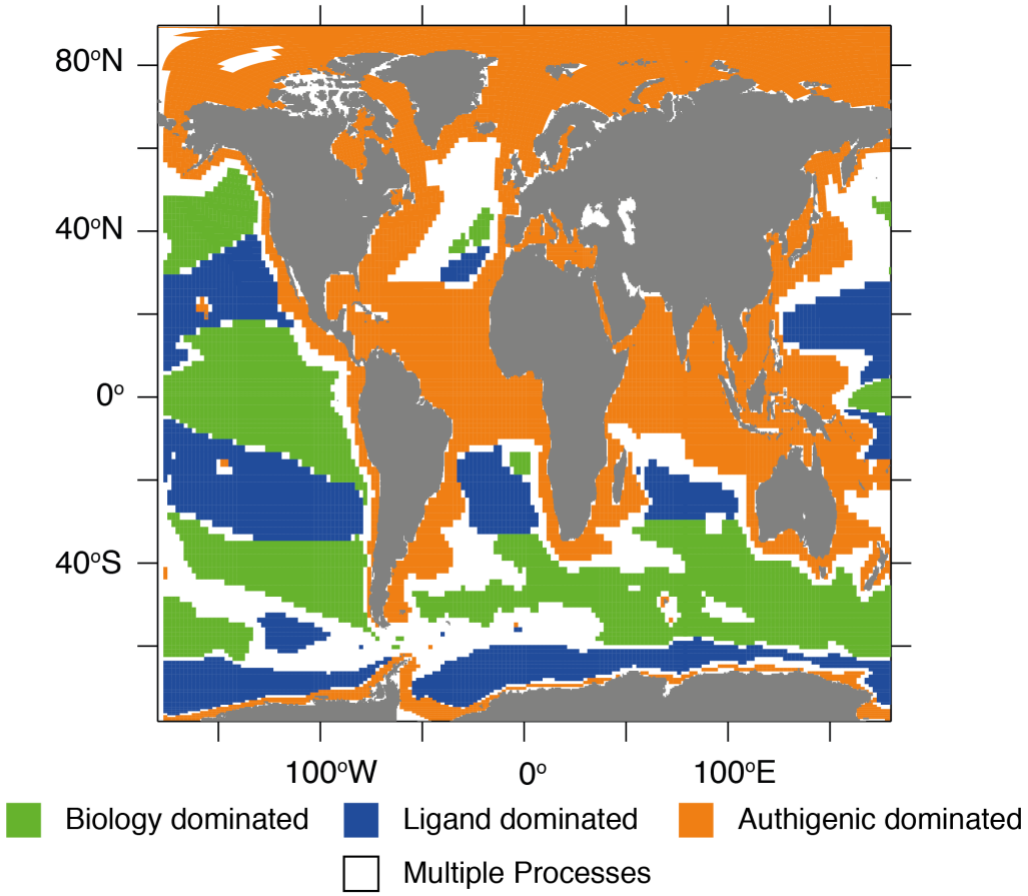
80°N
40°N
0°
40°S
100°W
0°
100°E
Biology dominated
Ligand dominated
Authigenic dominated
Multiple Processes

466
467

## Methods

The BAIT programme (GEOTRACES process study GApr13) conducted fieldwork as part of the BATS efforts during 2019. Water-column samples for analysis of iron and other trace metals were collected from the BATS site (31°40'N, 64°10'W) and adjacent BATS spatial stations during cruises in March (BAIT-I, spring), May (BAIT-II, early summer), August (BAIT-III, late summer) and November (BAIT-IV, autumn) 2019 aboard RV *Atlantic Explorer* and RV *Endeavor.* Seawater samples and associated hydrographic data were collected using a trace-metal clean conductivity-temperature-depth sensor (SBE 19 plus, SeaBird Electronics) mounted on a custom-built trace-metal clean carousel (SeaBird Electronics) fitted with custom-modified 5-L Teflon-lined external-closure Niskin-X samplers (General Oceanics), and deployed on an Amsteel non-metallic line. In addition, during the August cruise, near-surface samples (~1 m depth) were collected in a Niskin-X sampler that was hand-deployed from an inflatable dinghy ~500 m upwind of the research vessel, to avoid contamination from the ship. Upon recovery, Niskin-X samplers were transferred into a shipboard Class-100 clean-air laboratory, where seawater samples were filtered through pre-cleaned 0.2-µm pore AcroPak Supor filter capsules (Pall) using filtered nitrogen gas[9].

For DFe analysis, filtrate was collected in acid-cleaned 125 mL low-density polyethylene bottles (Nalgene). For analysis of Fe-binding ligands, filtrate was collected in acid-cleaned and Milli-Q-conditioned fluorinated polyethylene bottles and frozen at 20ºC until analyzed at the University of South Florida by competitive ligand exchange-adsorptive cathodic stripping voltammetry (CLE-AdCSV)[20]. For sFe measurements, the 0.2-µm filtrate was then filtered through dilute-acid-cleaned, sample-rinsed 0.02 µm Anotop syringe filters using a peristaltic pump; the resulting filtrate was stored in acid-cleaned 60 mL LDPE bottles and acidified to pH 1.7 post-cruise as for DFe samples. For analysis of particulate iron and other trace metals, 2.35-4.05 L of seawater were filtered through 25 mm diameter 0.45 µm polyethersulfone Supor membranes. The filters were cut in half for parallel analysis of labile and total particulate concentrations following the digestion methods of ref[50], and digested samples were analyzed by high-resolution ICP-MS following published protocols. Cellular iron contents of autotrophic flagellates from 20 m and the DCM were analyzed following published methods[51] at the Advanced Photon Source, Argonne National Laboratory microprobe beamline 2-ID-E. Our observations of ligands are consistent with previous measurements[21,22].

DFe and SFe were determined in the water-column samples using high-resolution inductively-coupled plasma mass spectrometry (HR-ICP-MS, Thermo Fisher Scientific ElementXR) with in-line separation-preconcentration (Elemental Scientific SeaFAST SP3). Calibration standards were prepared in low-iron seawater, for which initial DFe and SFe concentrations were determined using the method of standard additions, with yttrium used as an internal standard. Analytical blank concentrations were assessed by applying the in-line separation-preconcentration procedure including all reagents and loading air in place of the seawater sample ('air blank'), yielding a mean blank concentration that was not statistically different from zero (-0.006 ± 0.0178 nM, n = 62); the limit of detection, defined as the concentration equivalent to three times the standard deviation on the mean blank, was 0.054 nM Fe. The mean DFe concentration for ten separate determinations of the GEOTRACES GSP seawater consensus material was 0.177 ± 0.030 nM, which is within analytical uncertainty (one sigma) of the current consensus value 0.155 ± 0.045 nM DFe. Estimated analytical precision for DFe at the GSP concentration level is ± 17% (± one sigma, n = 10), and generally better than ±10% based on repeat determinations for samples with DFe concentrations greater than 0.2 nM. CFe was calculated as the difference between DFe and SFe.

The particulate Fe pool was partitioned into lithogenic, authigenic, and biogenic phases using direct measurements of the biogenic fraction, Al tracer to estimate the lithogenic fraction, and a well-characterized chemical leach for labile material. Biogenic PFe was calculated from the measured seasonal mean cellular Fe/C ratios, reported mean C:P at BATS, and measured labile particulate phosphorus: $PFe_{bio} = Fe{:}C \times C{:}P_{ref} \times PP_{labile}$. The use of a chemical leach for labile

material enabled us to define lithogenic PFe operationally as the measured refractory material, $PFe_{litho} = max(0, PFe_{total} - Fe_{labile})$. We compared this to the more commonly used approach of using aluminum as a proxy for lithogenic material, $PFe_{litho} = PAl_{total} \times Fe{:}Al_{ref}$, using two reference Fe:Al molar ratios – the mean of all upper continental crust (0.23 ref[52]) and Saharan dust aerosol (0.42, ref[53]). The remaining PFe was defined as authigenic: $PFe_{auth} = max(0, PFe_{total} - PFe_{litho} - PFe_{bio})$.

We also used the 2021 GEOTRACES intermediate data product (IDP2021)[54] to explore the potential importance of authigenic Fe. We used the IDP2021 observations of labile PFe (assuming that this reflects the actively cycling PFe pool and generally excludes lithogenic PFe) and sought to address whether this pool could be accounted for solely by the commonly considered biogenic PFe pool. To do so we used IDP2021 labile particulate phosphorus data and a high or low estimate of Fe/P cellular quotas (40 and 10 mmol Fe / mol P). When these different estimates of biogenic PFe were subtracted from the labile PFe, residual or 'missing' PFe was present in half to three-quarters of observations. To avoid biases associated with margin sediments and hydrothermal vents, we conducted this analysis in waters shallower than 2000m at stations where bottom depths exceeded 3000m depth.

**Model Equations:**

Our modelling is based on 'quota' version of the well-established PISCES-v2 model that forms part of the IPSL earth system model.

*PISCES-Quota* - This follows the standard PISCES Quota code[55], including three phytoplankton groups (picophytoplankton, nanophytoplankton and diatoms), fully decoupled carbon, nitrogen, phosphorus, silica and iron stoichiometry within phytoplankton, dissolved organic and particle pools, with the addition of two aeolian derived lithogenic particle tracers (fine lithogenic particles and aggregated lithogenic particles) following[56]. Fine lithogenic particles sink at 0.5 m $d^{-1}$ and aggregate to form aggregated lithogenic particles which sink at 10 m $d^{-1}$ and disaggregate. The Fe chemistry routines in the *PISCES-Quota* code assume all DFe is in equilibrium with ligands (Figure 2b) and has two minor alterations from the standard PISCES-v2 code[57]: (1) Weak total ligands ($L_T$) are derived from modelled DOC using a default ratio of 0.09 nM $L_T$ (mmol DOC $m^{-3})^{-1}$ (with extra experiments at 0.08 and 0.07 nM $L_T$ (mmol DOC $m^{-3})^{-1}$) and (2) use a fixed log conditional stability constant of 11 to approximate the weaker total ligand pool[2]. *PISCES-Quota* is also run with prognostic stronger L1 ligands (see below). In PISCES-Quota CFe may aggregate (AGG), with a constant stickiness (S) parameter of 0.3, as per the standard PISCES code:

$$AGG = (A*DOC + B*POC_S)*shear + C*POC_S + D*DOC + E*POC_S + (F*shear + G)*POC_L \quad (1)$$

Where, A = 12.0*S, B = 9.05, C = 2.49, D = 127.8*S, E = 725.7, F = 1.94 and G = 1.37 (all constants are in $(mol\ C/L)^{-1}\ s^{-1}$ and from the original PISCES model[57]). $POC_S$ and $POC_L$ refer to small and large particulate organic carbon, respectively. In PISCES-Quota, CFe is assumed to be a fixed 50% component of the FeL pool that dominates DFe[57]. Shear is set to 1 in the mixed layer and 0.01 below.

Aeolian inputs of DFe and fine lithogenic particles are from a 1980-2015 monthly aerosol climatology[58].

*PISCES-Quota-Fe* – this builds on *PISCES-Quota*, but adds two additional particulate authigenic tracers (small and large particulate authigenic Fe). Representing the cycling of colloidal Fe (oxyhydr)oxides out of equilibrium with ligands also required a number of modifications to the Fe chemistry routine.

Empirical calculation of Fe solubility following experimental data[59] defines soluble Fe (SFe). Any DFe in excess of the SFe concentration is assumed to be made up of colloidal Fe (oxyhydr)oxides (CFe or FeOX). This now means that FeOX can vary beyond the fixed contribution to DFe assumed previously, consistent with observations. We assume FeOX makes a minimum of 10% of DFe. SFe can be complexed by ligands (see below) to produce SFeL, with uncomplexed SFe (SFe') participating in the standard PISCES particle scavenging process (with organic and lithogenic particles, Figure 2c).

The rate of change in small particulate authigenic Fe (aFeS):

D(aFeS)/dt = FeOX*AGG + FeOX*AUTO – aFeS_agg*aFeS - aFeS_agg2*aFeL – aFeS_diss*aFeS + aFeL_disagg*aFeL (2)

AGG is the specific rate of FeOX aggregation from the standard PISCES routines[57], as per equation 1 aggregation of FeOX is driven by DOC and POC concentrations (aggregation/coagulation with DOC is increased 3-fold, collf=3). Interaction of FeOX with DOC is modulated by an assumed background stickiness of DOC (S, 0.3) and the relative concentration of living biomass (Rbio = Tbio/(Tbio+kbtbio), Tbio is the sum of all living phytoplankton and kbtbio = 3.E-8 mol/L) as proxy for stickier DOC. Constants modified from equation 1 are: A = 12.0*S*collf*Rbio and D = 127.8*S*collf*Rbio (all constants are in $(mol\ C/L)^{-1}\ s^{-1}$).

AUTO is an additional specific rate that accounts for the autocatalytic aggregation of FeOX at high concentrations. It is calculated based on a standard FeOX aggregation rate (0.1 $d^{-1}$, FeOX_agg) and a shape function of kcfe = 2nM:

AUTO = FeOX_agg * FeOX^4 / ( FeOX^4 + kcfe^4) (4)

Removal of FeOX via both aggregation with organic carbon and autocatalytic aggregation is a sink for DFe and a source for small authigenic particles (aFeS).

aFeS is lost by autocatalytic aggregation (aFeS_agg, accounting for shear) and by interaction with large authigenic Fe (aFeS_agg2, not including shear) to form aFeL following the assumptions in the standard PISCES particle code.

aFeS sinks at 0.5 m $d^{-1}$ and aFeS dissolution (aFeS_diss) set to 1.E-4 $d^{-1}$.

Rate of change in aFeL:

D(aFeL)/dt = aFeS_agg*aFeS + aFeS_agg2*aFeL - aFeL_disagg*aFeL - aFeL_diss*AFeL (5)

And accounts for aggregation of AFeS (see above) and the disaggregation (aFeL_disagg, 1.E-3 $d^{-1}$). aFeL sinks at 10 m $d^{-1}$.

*Ligands* - Both PISCES-Quota and PISCES-Quota-Fe can be run with either weaker total ligands ($L_T$, derived from DOC and a fixed log conditional stability constant of 11) or using the prognostic ligand model for stronger $L_1$ ligands (with a fixed log conditional stability constant of 12). The prognostic $L_1$ model is used by PISCES-Quota-Fe as default and based on the standard PISCES ligand model[44], with small adjustments to parameter values. Minimum and maximum lifetimes of $L_1$ ligands are set to 0.2 and 100 years. The production rates of L1 ligands from phytoplankton DOC production, zooplankton DOC production and detritus remineralisation are set to 1.E-4, 1.E-5 and 5.E-5 mol $L_1$ mol $C^{-1}$, respectively. Photochemical loss of $L_1$ ligands is set to 1.E-4 $(W\ m^{-2})^{-1}\ d^{-1}$, modulated by a shape function of 1.E-9 mol $L_1$ $L^{-1}$. These changes were made to maximise the fit between the modelled and observed $L_1$ ligands (Extended Data Figure 1).

Model DFe and PFe distributions were compared to the GEOTRACES IDP2021 dataset[54]. Observations were binned onto the model grid and linear regression analysis was performed after log transformation, as in previous model-data assessments[13]. Observations and model solutions for PISCES-Quota and PISCES-Quota-Fe are compared in Extended Data Figure 4 for ten GEOTRACES ocean transects. We also compared how the PISCES-Quota model solution compared to the standard version of PISCES in terms of its ability to reproduce the seasonal variations in DFe in Extended Data Figure 3.

**Additional References**


50 Rauschenberg, S. & Twining, B. S. Evaluation of approaches to estimate biogenic particulate trace metals in the ocean. *Marine Chemistry* **171**, 67-77, doi:10.1016/j.marchem.2015.01.004 (2015).

51 Twining, B. S. *et al.* Taxonomic and nutrient controls on phytoplankton iron quotas in the ocean. *Limnology and Oceanography Letters*, doi:10.1002/lol2.10179 (2020).

52 Rudnick, R. L. & Gao, S. Composition of the Continental Crust. *Treatise on Geochemistry*, 1-64, doi:10.1016/b0-08-043751-6/03016-4 (2003).

53 Shelley, R. U., Morton, P. L. & Landing, W. M. Elemental ratios and enrichment factors in aerosols from the US-GEOTRACES North Atlantic transects. *Deep Sea Research Part II: Topical Studies in Oceanography* **116**, 262-272, doi:10.1016/j.dsr2.2014.12.005 (2015).

54 The GEOTRACES Intermediate Data Product 2021 (IDP2021). *NERC EDS British Oceanographic Data Centre NOC*, doi:10.5285/cf2d9ba9-d51d-3b7c-e053-8486abc0f5fd.

55 Kwiatkowski, L., Aumont, O., Bopp, L. & Ciais, P. The impact of variable phytoplankton stoichiometry on projections of primary production, food quality and carbon uptake in the global ocean. *Global Biogeochemical Cycles*, doi:10.1002/2017gb005799 (2018).

56 Ye, Y. & Völker, C. On the Role of Dust-Deposited Lithogenic Particles for Iron Cycling in the Tropical and Subtropical Atlantic. *Global Biogeochemical Cycles* **31**, 1543-1558, doi:10.1002/2017gb005663 (2017).

57 Aumont, O., Ethé, C., Tagliabue, A., Bopp, L. & Gehlen, M. PISCES-v2: an ocean biogeochemical model for carbon and ecosystem studies. *Geoscientific Model Development* **8**, 2465-2513, doi:10.5194/gmd-8-2465-2015 (2015).

58 Hamilton, D. S. *et al.* Recent (1980 to 2015) Trends and Variability in Daily-to-Interannual Soluble Iron Deposition from Dust, Fire, and Anthropogenic Sources. *Geophysical Research Letters* **47**, doi:10.1029/2020gl089688 (2020).

59 Liu, X. & Millero, F. J. The solubility of iron in seawater. *Marine Chemistry* **77**, 43-54, doi:10.1016/s0304-4203(01)00074-3 (2002).

## Extended Data

**Extended Data Figure 1**. **Seasonal evolution of total and stronger ligands** Observed and modelled total (black symbols) and stronger (red symbols) ligand concentrations (nM). Black lines are model solutions at BATS from the PISCES-Quota model, with varying total ligands derived from DOC (using 0.09, 0.08 and 0.07 nM LT µM $DOC^{-1}$). Blue lines represent model solutions from PISCES-Quota-Fe, with either prognostic stronger ligands (solid blue) or DOC-derived total weaker ligands (Blue dashed, using 0.09 nM LT µM $DOC^{-1}$).

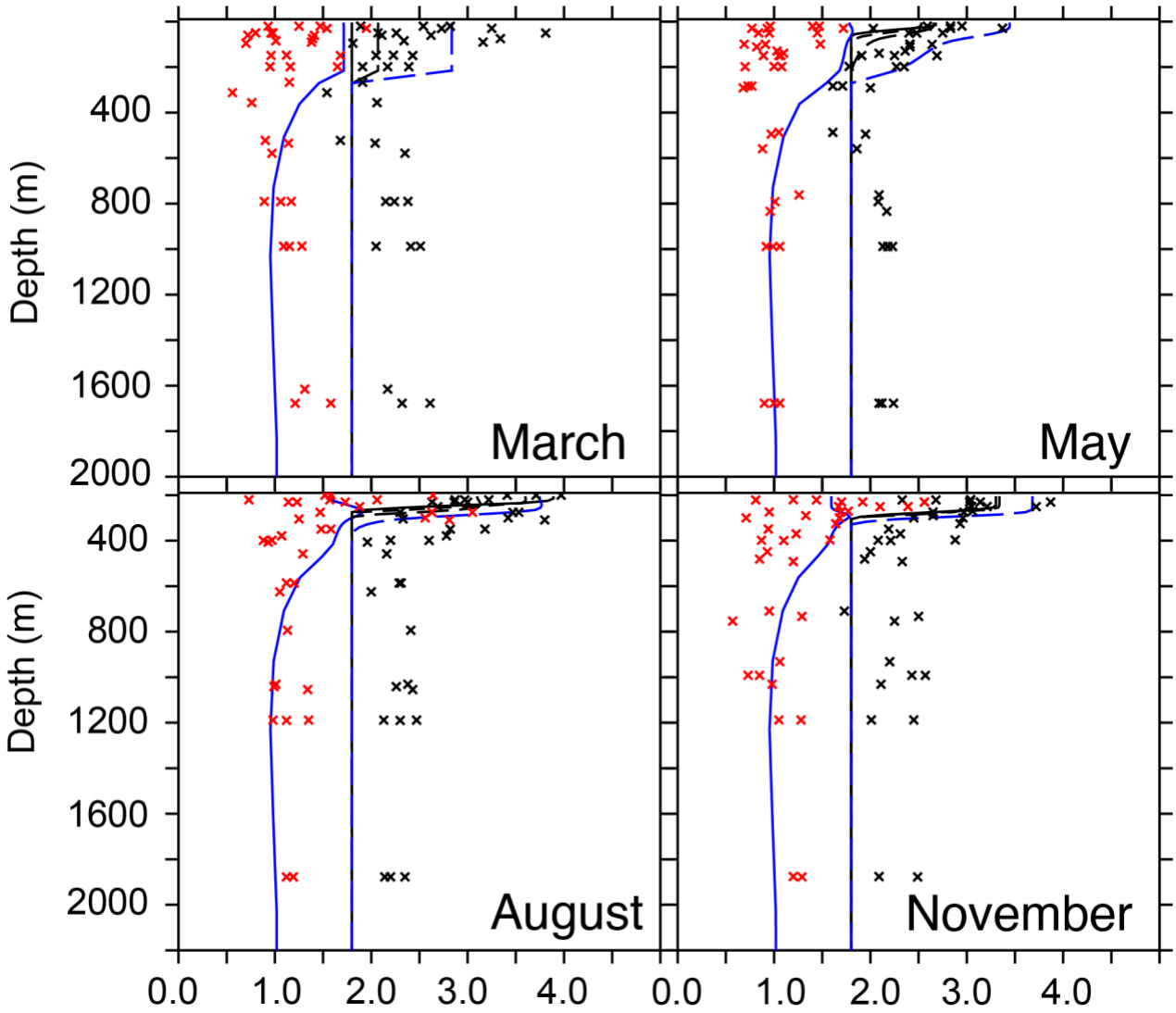

**Extended Data Figure 2**. **Seasonal evolution of excess ligands** Observed and modelled excess total (black symbols) and strong (red symbols) ligands (both in nM). Thick and dashed black lines are model solutions at BATS from the PISCES-Quota model, with varying total ligands derived from DOC (using 0.09, 0.08 and 0.07 nM Lt µM $DOC^{-1}$) or prognostic stronger ligands (thin black lines). Blue lines represent model solutions from PISCES-Quota-Fe, with either prognostic stronger ligands (solid blue) or DOC-derived total ligands (Blue dashed, using 0.09 nM Lt µM $DOC^{-1}$). Values less than zero are when DFe concentrations exceed the concentrations of either L1 or LT. Only the PISCES-Quota-Fe model is able to generate the observed large excess ligand pools.

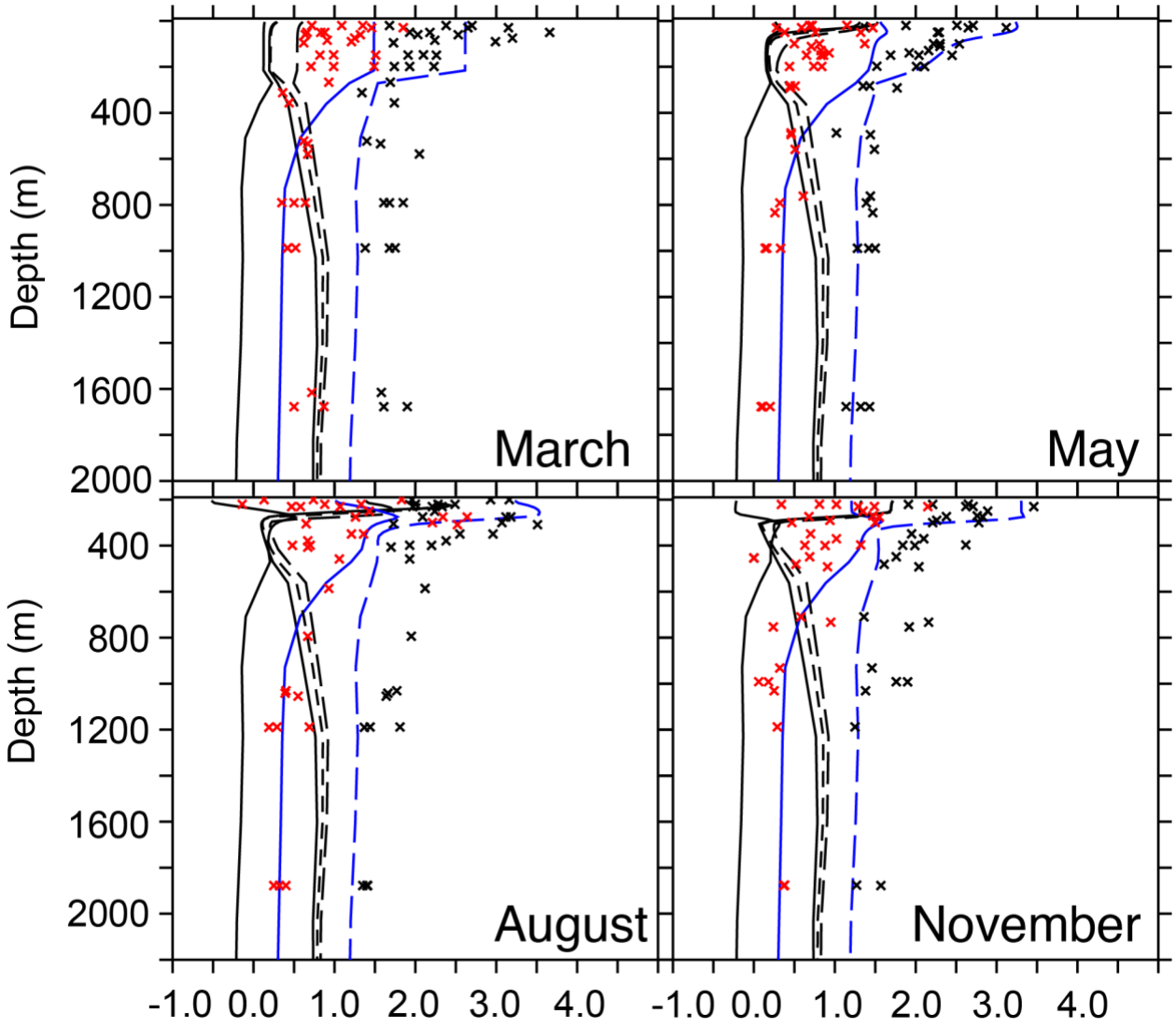

**Extended Data Figure 3. Variations in the seasonal evolution of dissolved iron**. DFe data and model solutions at the BATS site. Red crosses are DFe data for each voyage for three stations in the BATS region. All black lines are model solutions at BATS from the PISCES-Quota model, with total ligands derived from DOC (using 0.09 (nM Lt) (µM DOC)$^{-1}$) but with varying strengths of scavenging of free Fe by lithogenic particles. Blue lines represent model solutions from the new PISCES-Quota-Fe, with either prognostic stronger ligands (solid blue) or DOC-derived total ligands (Blue dashed, using 0.09 (nM Lt) (µM DOC)$^{-1}$). In red, we also compare the default PISCES-Quota (solid red, with total ligands derived from DOC using 0.09 (nM Lt) (µM DOC)$^{-1}$) and PISCES standard (red dashed) models. This demonstrates that there is little difference in the model-data mismatch in the seasonal evolution of DFe between PISCES-Quota and the standard PISCES model.

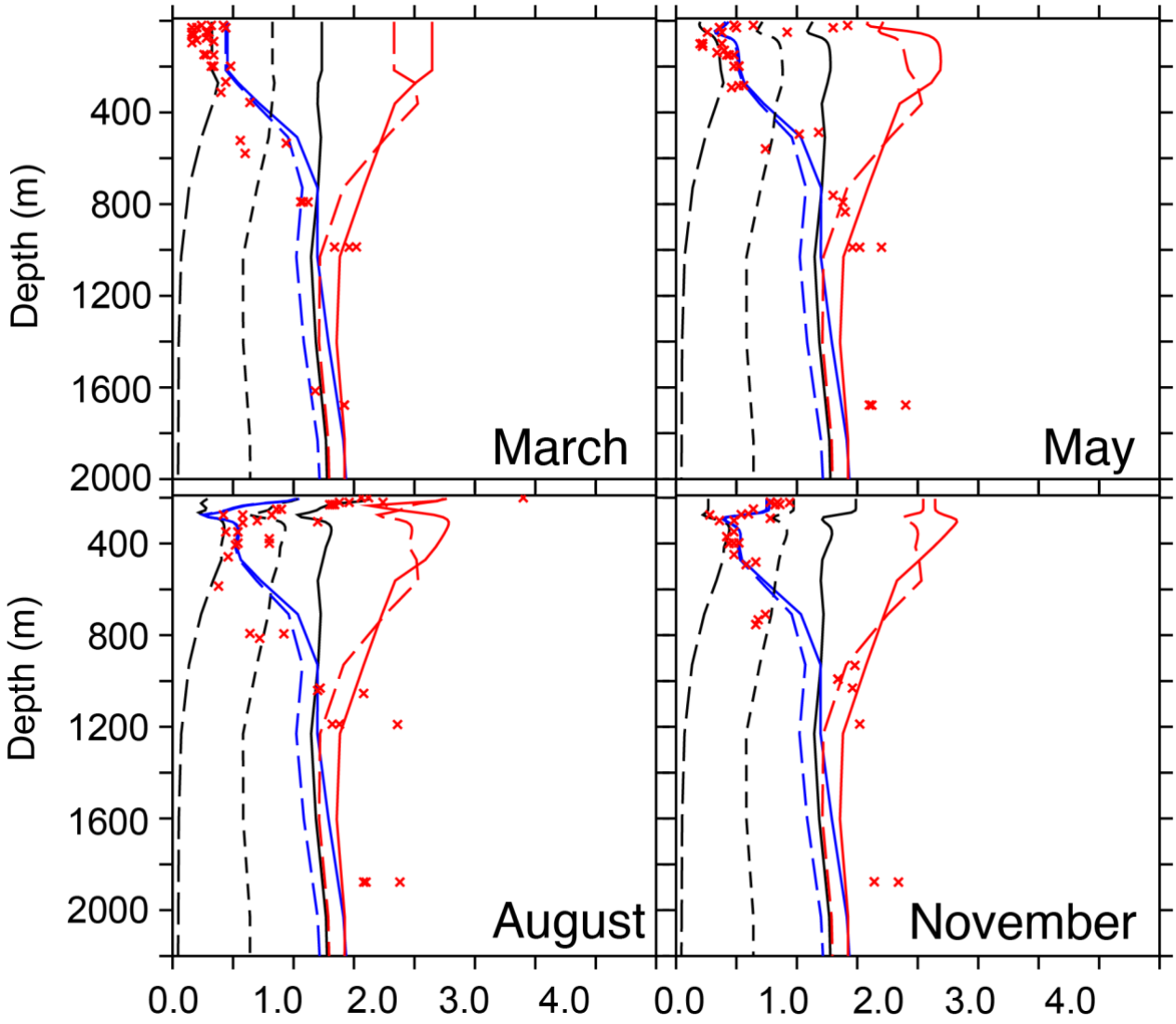

**Extended Data Figure 4**. **Global model-data comparison of dissolved iron** Observed and modelled dissolved iron (nM) for ten GEOTRACES sections for PISCES-Quota-Fe and PISCES-Quota. Observations and models are binned onto the same vertical grid.

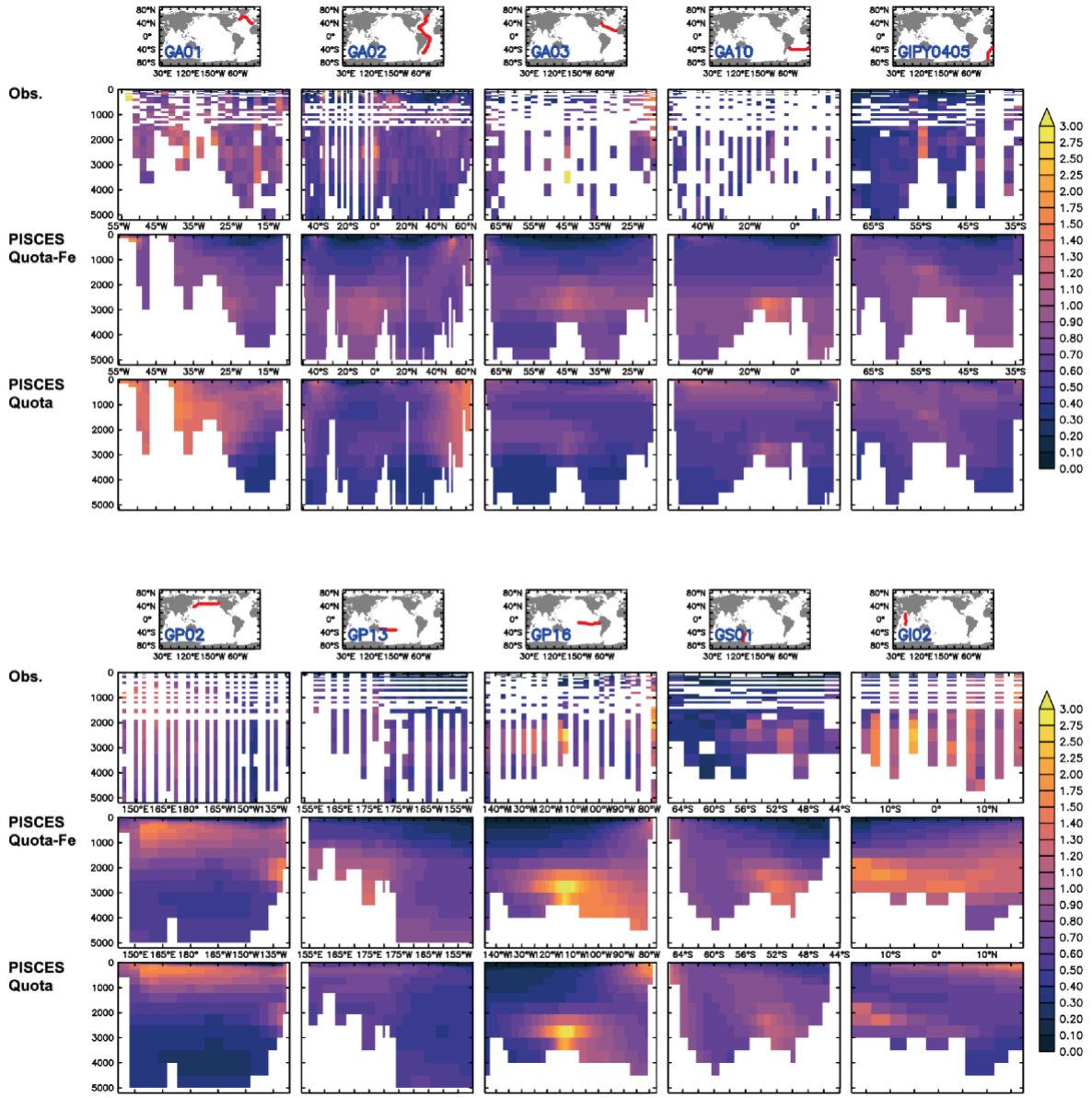

**Extended Data Figure 5**. **Model performance for biogeochemical metrics** Plots showing the difference in performance between PISCES-Quota and PISCES-Quota-Fe for a suite of biogeochemical diagnostics. Average upper 100m $NO_3$ and $PO_4$ are in mmol $m^{-3}$, average 200-600m $O_2$ is in mmol $m^{-3}$, total chlorophyll (T-Chl) at the surface (summed across the picophytoplankton, nanophytoplankton and diatoms) is in mg $m^{-3}$, and carbon export at 100m is in mol $m^{-2}$ $yr^{-1}$. It can be seen that the new PISCES-Quota-Fe model does not significantly alter the biogeochemical mean state of the model.

$NO_3$ (0–100m), PISCES–Quota PISCES–Quota–Fe

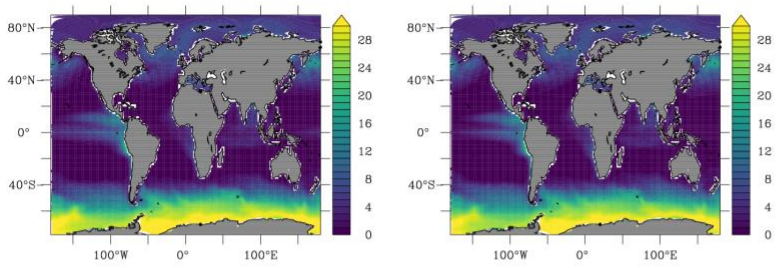


$PO_4$ (0–100m), PISCES–Quota PISCES–Quota–Fe

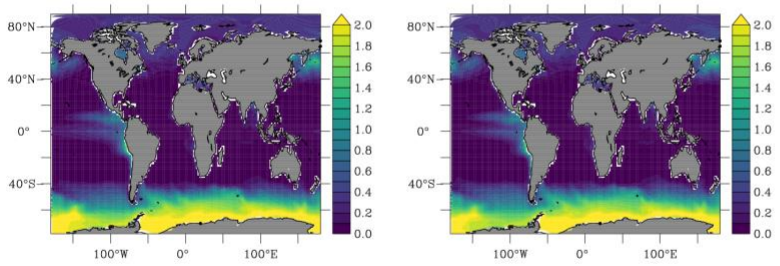


$O_2$ (200–600m), PISCES–Quota PISCES–Quota–Fe

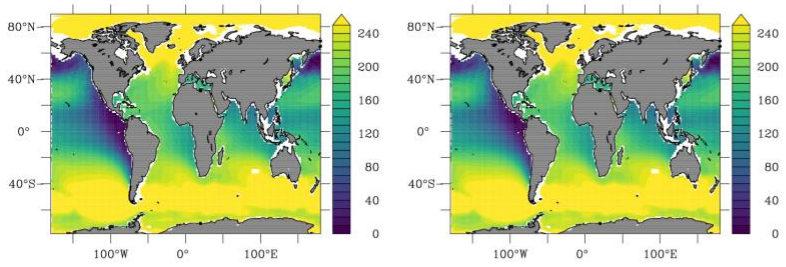


T–Chl, PISCES–Quota PISCES–Quota–Fe

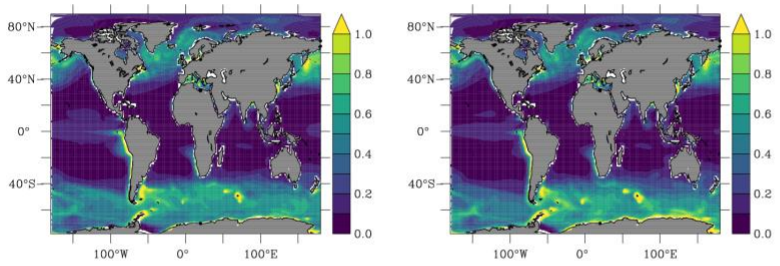


Cexp (100m), PISCES–Quota PISCES–Quota–Fe

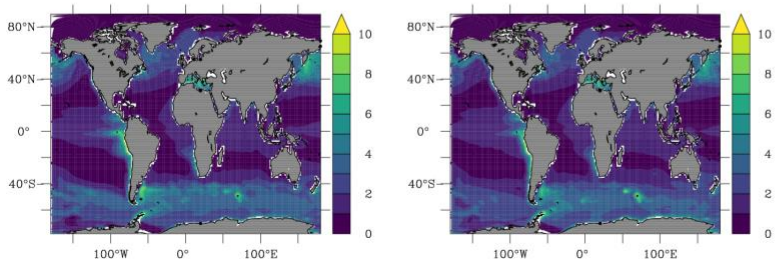


716
717
718

**Extended Data Figure 6. Iron cycle fluxes in the Atlantic and Pacific Oceans** Proportional contributions of different processes to total DFe supply and removal fluxes along two example sections in the Atlantic (20W) and Pacific (150W) oceans from the PISCES-Quota-Fe model with prognostic strong ligands.

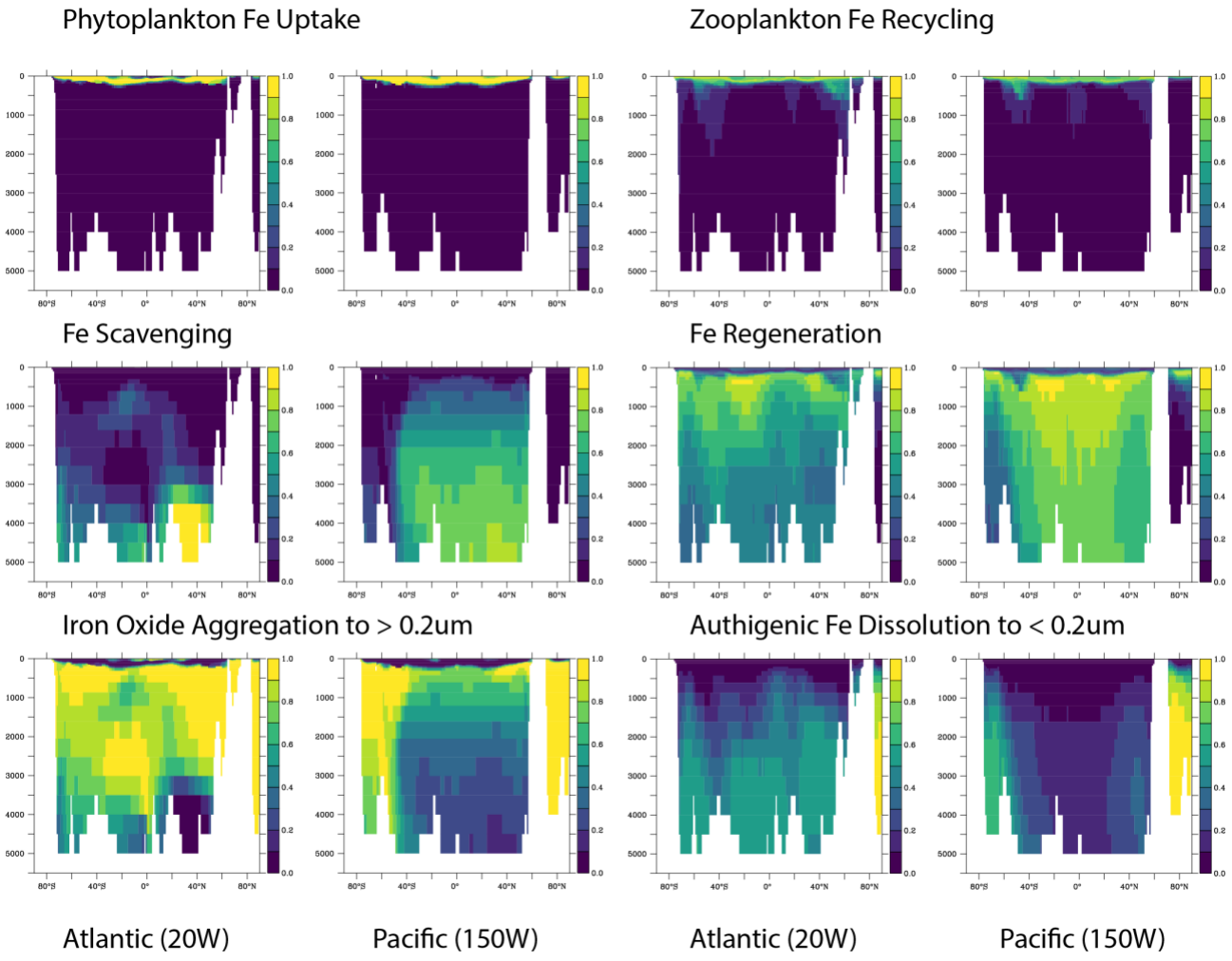

**Extended Data Table 1. Prior iron cycle process studies** A summary of available measurements of the ocean iron cycle from time series stations and process studies that collected temporal observations. We provide the name and broad location and year of the study, the seasonal sampling frequency, depths and whether there was concurrent sampling of dissolved Fe (DFe), particulate iron (PFe), total ligands ($L_{tot}$), strong and weak ligands (L1 and L2), and PFe phases (lithogenic and biogenic). The current study, in the top row, is the only one to provide such data across all seasons and iron parameters.

| Name / Location | Sampling frequency | | | | | Depths | dFe | pFe | $L_{tot}$ | L1,L2 | pFe phases | | References |
|---|---|---|---|---|---|---|---|---|---|---|---|---|---|
| | Year | Winter | Spring | Summer | Autumn | | | | | | Lithogenic Fe | Biogenic Fe | |
| **BATS** | 2019 | x | x | x | x | All | x | x | x | x | x | x | This study |
| *NW Atlantic (near Bermuda)* | 2011 | | | | x | All | | | | | | | 1–4 |
| | 2010 | | | x | | All | | | | | | | 5,6 |
| | 2008 | | x | x | x | All | | | | | | | 7 |
| | 2007 | | x | x | x | All | x | | | (x) | | | 7 |
| | 2004 | | x | | | 0-1000m | x | | | | | | 8 |
| | 2003 | | | x | | 0-1000m | x | | | | | | 8 |
| **DYFAMED** | (2005-)2006 | x | x | x | x | Surface | x | | x | | | | 9 |
| *NW Mediterranean* | 2004(-2005) | x | x | x | x | Surface | x | | | | | | 10 |
| | 1999 | | | | x | All | x | | | | | | 11 |
| | 1995 | | x | | | 0-1500m | x | x | | | x | | 12 |
| | 1994 | | | | x | 0-1000m | x | x | | | x | | 12 |
| **HOT** | 2015 | | | x | | 0-400m | x | | x | | | | 13 |
| *NW Pacific (near Hawaii)* | 2013 | | x | x | x | Surface | x | (x) | (x) | | | | 14 |
| | | | | x | x | 0-1400m | x | | (x) | | | | 14 |
| | 2012 | | x | x | x | Surface | x | x | (x) | | | | 14 |
| | | | x | x | | 0-1400m | x | | (x) | | | | 14 |
| | 2005 | | x | | | All | x | | | | | | 15 |
| | 2002 | | | x | x | Surface | x | | | | | | 16 |
| | | | | x | | All | x | | | | | | 16,17 |
| | 2001 | | x | | | All | x | | (x) | | | | 16,18 |
| | 1999 | | x | | | Surface | x | | | | | | 16 |
| | 1998 | | | | x | Surface | x | | | | | | 16 |
| | 1994 | x | | | | 0-2000m | x | | | x | | | 19 |
| **Station P** | 2013 | | | x | | 0-2000m | x | | | | | | 20 |
| *NE Pacific* | 2012 | | | x | | 0-2000m | x | | | | | | 20 |
| | 2007 | | x | | | 0-180m | x | | | | | | 21 |
| | 2006 | | | x | | 0-180m | x | | | | | | 21 |
| | 2001 | x | | | | 0-1000m | x | | | | | | 22 |
| | 1999 | x | | | | 0-1000m | x | | | | | | 23 |
| | 1998 | x | | x | x | 0-800m | x | | | | | | 23 |
| | 1997 | | | | x | 0-600m | x | | | | | | 23 |
| | 1987 | | | x | | All | x | | | | x | | 24 |

| | | | | | | | | | | | | | |
|---|---|---|---|---|---|---|---|---|---|---|---|---|---|
| **SOTS** *Southern Ocean* | 2018 | | x | | | All | x | x | | | | | 25 |
| | 2016 | | | | x | 0-1500m | x | | | | | | 26 |
| **MOTS** *SW Pacific* | 2008 | | | x | x | Surface | x | | | x | | | 27 |
| | 2007 | | x | | | Surface | x | | | x | | | 27 |
| | 2005 | | | x | | Surface | x | | x | | | | 27 |
| | 2004 | | x | | x | Surface | x | | x | | | | 27 |
| | 2003 | x | x | x | x | Surface | x | | x | | | | 27 |
| | 2002 | x | x | | x | Surface | x | | x | | | | 27 |
| | 2000 | | x | | | Surface | | | | | | | 27 |
| **RaTS** *Southern Ocean (West Antarctic Peninsula)* | 2014 | | | x | | 0-75m | x | | | | | | 28 |
| | 2013 | | x | x | x | 0-75m | x | | | | | | 28 |
| | (2009-)2010 | | | x | x | Surface | x | | | | | | 29 |
| | 2010 | | | x | x | 0-200m | x | | | | | | 29 |
| **FeCycle II** *SW Pacific* | 2008 | | x | | | Surface (mostly) | x | x | | | x | x | 30,31 |
| **FeCycle I** *Southern Ocean* | 2003 | | | x | | Surface (mostly) | x | x | x | | x | x | 32–34 |
| **NE Atlantic** *near Cape Verde* | 2006 | x | | | | Surface | x | | x | | | | 35 |
| **NW Pacific** *California curr.* | 2007 | | x | | | Surface | x | | | x | | | 36 |
| | 2006 | | x | | | Surface | x | | | x | | | 36 |

x – season or parameter sampled
(x) – parameter only sampled during some occupations

References for


1. Hatta, M. *et al.* An overview of dissolved Fe and Mn distributions during the 2010-2011 U.S. GEOTRACES north Atlantic cruises: GEOTRACES GA03. *Deep. Res. Part II Top. Stud. Oceanogr.* **116**, 117–129 (2015).
2. Buck, K. N., Sohst, B. M. & Sedwick, P. N. The organic complexation of dissolved iron along the U.S. GEOTRACES (GA03) North Atlantic Section. *Deep. Res. Part II Top. Stud. Oceanogr.* **116**, 152–165 (2015).
3. Ohnemus, D. C. & Lam, P. J. Cycling of lithogenic marine particles in the US GEOTRACES North Atlantic transect. *Deep. Res. Part II Top. Stud. Oceanogr.* **116**, 283–302 (2015).
4. Lam, P. J., Ohnemus, D. C. & Auro, M. E. Size-fractionated major particle composition and concentrations from the US GEOTRACES North Atlantic Zonal Transect. *Deep. Res. Part II Top. Stud. Oceanogr.* **116**, 303–320 (2015).
5. Gerringa, L. J. A., Rijkenberg, M. J. A., Schoemann, V., Laan, P. & de Baar, H. J. W. Organic complexation of iron in the West Atlantic Ocean. *Mar. Chem.* **177**, 434–446 (2015).
6. Rijkenberg, M. J. A. *et al.* The distribution of dissolved iron in the West Atlantic Ocean. *PLoS One* **9**, 1–14 (2014).
7. Sedwick, P. N. *et al.* Dissolved iron in the Bermuda region of the subtropical North Atlantic Ocean: Seasonal dynamics, mesoscale variability, and physicochemical speciation. *Mar. Chem.* **219**, (2020).
8. Sedwick, P. N. *et al.* Iron in the Sargasso Sea (Bermuda Atlantic Time-series Study region) during summer: Eolian imprint, spatiotemporal variability, and ecological implications. *Global Biogeochem. Cycles* **19**, (2005).
9. Wagener, T., Pulido-Villena, E. & Guieu, C. Dust iron dissolution in seawater: Results from a one-year time-series in the Mediterranean Sea. *Geophys. Res. Lett.* **35**, 1–6 (2008).
10. Bonnet, S. & Guieu, C. Atmospheric forcing on the annual iron cycle in the western Mediterranean Sea: A 1-year survey. *J. Geophys. Res. Ocean.* **111**, 1–13 (2006).
11. Guieu, C. *et al.* Impact of high Saharan dust inputs on dissolved iron concentrations in the Mediterranean Sea. *Geophys. Res. Lett.* **29**, 2–5 (2002).
12. Sarthou, G. & Jeandel, C. Seasonal variations of iron concentrations in the Ligurian Sea and iron budget in the Western Mediterranean Sea. *Mar. Chem.* **74**, 115–129 (2001).

13. Bundy, R. M. *et al.* Distinct siderophores contribute to iron cycling in the mesopelagic at station ALOHA. *Front. Mar. Sci.* **5**, 1–15 (2018).
14. Fitzsimmons, J. N. *et al.* Daily to decadal variability of size-fractionated iron and iron-binding ligands at the Hawaii Ocean Time-series Station ALOHA. *Geochim. Cosmochim. Acta* **171**, 303–324 (2015).
15. Wu, J., Wells, M. L. & Rember, R. Dissolved iron anomaly in the deep tropical-subtropical Pacific: Evidence for long-range transport of hydrothermal iron. *Geochim. Cosmochim. Acta* **75**, 460–468 (2011).
16. Boyle, E. A., Bergquist, B. A., Kayser, R. A. & Mahowald, N. Iron, manganese, and lead at Hawaii Ocean Time-series station ALOHA: Temporal variability and an intermediate water hydrothermal plume. *Geochim. Cosmochim. Acta* **69**, 933–952 (2005).
17. Brown, M. T., Landing, W. M. & Measures, C. I. Dissolved and particulate Fe in the western and central North Pacific: Results from the 2002 IOC cruise. *Geochemistry, Geophys. Geosystems* **6**, (2005).
18. Wu, J., Boyle, E., Sunda, W. & Wen, L. S. Soluble and colloidal iron in the oligotrophic North Atlantic and North Pacific. *Science (80-. ).* **293**, 847–849 (2001).
19. Rue, E. L. & Bruland, K. W. Complexation of iron(III) by natural organic ligands in the Central North Pacific as determined by a new competitive ligand equilibration/adsorptive cathodic stripping voltammetric method. *Mar. Chem.* **50**, 117–138 (1995).
20. Schallenberg, C., Davidson, A. B., Simpson, K. G., Miller, L. A. & Cullen, J. T. Iron(II) variability in the northeast subarctic Pacific Ocean. *Mar. Chem.* **177**, 33–44 (2015).
21. Roy, E. G. & Wells, M. L. Evidence for regulation of Fe(II) oxidation by organic complexing ligands in the Eastern Subarctic Pacific. *Mar. Chem.* **127**, 115–122 (2011).
22. Johnson, W. K., Miller, L. A., Sutherland, N. E. & Wong, C. S. Iron transport by mesoscale Haida eddies in the Gulf of Alaska. *Deep. Res. Part II Top. Stud. Oceanogr.* **52**, 933–953 (2005).
23. Nishioka, J., Takeda, S., Wong, C. S. & Johnson, W. K. Size-fractionated iron concentrations in the northeast Pacific Ocean: Distribution of soluble and small colloidal iron. *Mar. Chem.* **74**, 157–179 (2001).
24. Martin, J. H., Gordon, R. M., Fitzwater, S. & Broenkow, W. W. Vertex: phytoplankton/iron studies in the Gulf of Alaska. *Deep Sea Res. Part A, Oceanogr. Res. Pap.* **36**, 649–680 (1989).
25. Barrett, P. M., Grun, R. & Ellwood, M. J. Tracing iron along the flowpath of East Australian Current using iron stable isotopes. *Mar. Chem.* **237**, 104039 (2021).
26. Ellwood, M. J. *et al.* Distinct iron cycling in a Southern Ocean eddy. *Nat. Commun.* **11**, 825 (2020).
27. Sander, S. G. *et al.* Spatial and seasonal variations of iron speciation in surface waters of the Subantarctic front and the Otago Continental Shelf. *Mar. Chem.* **173**, 114–124 (2015).
28. Bown, J. *et al.* Bioactive trace metal time series during Austral summer in Ryder Bay, Western Antarctic Peninsula. *Deep. Res. Part II Top. Stud. Oceanogr.* **139**, 103–119 (2017).
29. Annett, A. L. *et al.* Comparative roles of upwelling and glacial iron sources in Ryder Bay, coastal western Antarctic Peninsula. *Mar. Chem.* **176**, 21–33 (2015).
30. Boyd, P. W. *et al.* Microbial control of diatom bloom dynamics in the open ocean. *Geophys. Res. Lett.* **39**, 2–7 (2012).
31. Ellwood, M. J. *et al.* Pelagic iron cycling during the subtropical spring bloom, east of New Zealand. *Mar. Chem.* **160**, 18–33 (2014).
32. Boyd, P. W. *et al.* FeCycle: Attempting an iron biogeochemical budget from a mesoscale SF6 tracer experiment in unperturbed low iron waters. *Global Biogeochem. Cycles* **19**, 1–13 (2005).
33. Croot, P. L. *et al.* Physical mixing effects on iron biogeochemical cycling: FeCycle experiment. *J. Geophys. Res. Ocean.* **112**, 1–18 (2007).
34. Frew, R. D. *et al.* Particulate iron dynamics during FeCycle in subantarctic waters southeast of New Zealand. *Global Biogeochem. Cycles* **20**, 1–15 (2006).
35. Rijkenberg, M. J. A. *et al.* Changes in iron speciation following a Saharan dust event in the tropical North Atlantic Ocean. *Mar. Chem.* **110**, 56–67 (2008).
36. King, A. L., Buck, K. N. & Barbeau, K. A. Quasi-Lagrangian drifter studies of iron speciation and cycling off Point Conception, California. *Mar. Chem.* **128**–**129**, 1–12 (2012).

**Extended Data Table 2. Model-observations statistical assessment** Summary statistics for dissolved and particulate Fe across the PISCES-Quota-Fe and PISCES-Quota models for full depth and the upper 200m using data compiled from the 2021 GEOTRACES intermediate data product. We report the number of observations, model and observation mean (all in nM), bias, and the slope and correlation coefficient (R) for log transformed analysis. In all cases, PISCES-Quota-Fe has a lower bias, better correlation and displays a slope closer to 1.0, indicating improved performance. Persistent biases in PFe reflect missing additional lithogenic PFe sources.

| | Depths | Exp. | Nr. of obs. | Obs mean | Model mean | Bias | Slope | R |
|---|---|---|---|---|---|---|---|---|
| **DFe** | Full Depth | PISCES-Quota-Fe | 10743 | 0.37 | 0.43 | 0.06 | 0.8 | 0.59 |
| | | PISCES-Quota | | | 0.63 | 0.26 | 0.32 | 0.41 |
| | Upper 200m | PISCES-Quota-Fe | 4545 | 0.22 | 0.21 | -0.01 | 0.78 | 0.51 |
| | | PISCES-Quota | | | 0.56 | 0.34 | 0.45 | 0.49 |
| **PFe** | Full Depth | PISCES-Quota-Fe | 1664 | 0.85 | 0.48 | -0.37 | 0.7 | 0.59 |
| | | PISCES-Quota | | | 0.28 | -0.58 | 0.39 | 0.3 |
| | Upper 200m | PISCES-Quota-Fe | 687 | 0.66 | 0.38 | -0.28 | 0.48 | 0.47 |
| | | PISCES-Quota | | | 0.28 | -0.39 | 0.25 | 0.24 |